Rice LEAFY COTYLEDONE1 regulates embryonic envelope development and chlorophyll biogenesis in embryo

Chen Chen (chenchen@yzu.edu.cn)
Yangzhou University https://orcid.org/0000-0002-9748-3111
Baixiao Niu
Yangzhou University
Zongju Yang
Yangzhou University
Tianqi Bai
Yangzhou University
Zhiguo E
China National Rice Research Institute
Xinyu Xu
Yangzhou University
Qianbin Yun
Yangzhou University
Juan Zhang
Yangzhou University
Zhenyu Zhang
Yangzhou University
Xinming Lu
Yangzhou University
Qianfeng Li
Yangzhou University
Qiaoquan Liu
Yangzhou University https://orcid.org/0000-0001-5543-5798

Article

Keywords: chlorophyll biogenesis, plant genetics, embryonic envelope

Posted Date: September 22nd, 2021

DOI: https://doi.org/10.21203/rs.3.rs-888827/v1

Rice *LEAFY COTYLEDONE1* regulates embryonic envelope development and chlorophyll biogenesis in embryo

Baixiao Niu[1,†], Zongju Yang[1,†], Tianqi Bai[1,†], Zhiguo E[2], Xinyu Xu[1], Qianbin Yun[1], Juan Zhang[1], Zhenyu Zhang[1], Xinming Lu[1], Qianfeng Li[1], Qiao-Quan Liu[1], Chen Chen[1,*]

[1]Jiangsu Key Laboratory of Crop Genetics and Physiology/ Key Laboratory of Plant Functional Genomics of the Ministry of Education/ Jiangsu Key Laboratory of Crop Genomics and Molecular Breeding/ Jiangsu Co-Innovation Center for Modern Production Technology of Grain Crops, Agricultural College of Yangzhou University, Yangzhou, China

[2]Key Laboratory of Rice Biology, China National Rice Research Institute, Hangzhou, China

[†] These authors contributed equally to this work

[*] Correspondence: chenchen@yzu.edu.cn

Running title: OsNF-YB7 regulates rice embryo development

Abstract

The scutellum, coleoptile, coleorhiza, and epiblast (if it exists) consist of a complex embryonic envelope to protect the plumule and radicle inside a grass embryo. Controversies have been provoked for centuries regarding homologies of the grass embryonic structures. Here we found that the rice *LEAFY COTYLEDONE1* (*LEC1*) gene, *OsNF-YB7*, is vital for embryo development. A leaf-like structure (LL) was developed from the scutellum of *osnf-yb7* to replace the embryonic envelope that formed in wild-type. Additionally, *osnf-yb7* developed chloroembryos due to overactivated chlorophyll biosynthesis. Thus, OsNF-YB7 likely plays a dual role in chlorophyll biogenesis in rice embryos: (1) OsNF-YB7 directly represses genes, such as rice *GOLDED-LIKE1* (*OsGLK1*), involving chlorophyll biosynthesis; (2) OsNF-YB7 binds to OsGLK1 to repress the downstream genes of OsGLK1. Parallel phenotypes shown in *osnf-yb7* and *lec1* suggest functional conservation of the LEC1-type genes in plants. Both *lec1* cotyledons and *osnf-yb7* LL displayed true leaf characteristics. Our morphological and transcriptional evidence implied that LL replaces the embryonic envelope in *osnf-yb7*, raising the hypothesis that the grass embryonic envelope is an analog of Arabidopsis cotyledon. This study demonstrates that OsNF-YB7 acts as a negative regulator in chlorophyll biogenesis and is important for embryonic envelope formation.

Introduction

LEAFY COTYLEDON1 (*LEC1*) of Arabidopsis encodes a subunit of the nuclear family Y (NF-Y) transcription factor (TF) with specialized function in plants (Lotan et al., 1998; Lee et al., 2003). LEC1 and the B3 family TFs, including LEC2, ABA INSENSITIVE3 (ABI3), and FUSCA3 (FUS3), consist of a central hub for regulating the network of seed maturation (Jo et al., 2019; He and Niu, 2019; Lepiniec et al., 2018). Loss-of-function of *LEC1* results in desiccation intolerance, defects of storage macromolecule accumulation, activation of the shoot apices, and precocious germination (Meinke, 1992; Meinke et al., 1994; West et al., 1994; Mu et al., 2008; Harada, 2001). *LEC1* is also involved in Arabidopsis embryogenesis (Hu et al., 2018). The suspensor of the *lec1* embryo had more cells due to abnormal cell division (Meinke, 1992; Meinke et al., 1994; West et al., 1994); trichomes, the unicellular outgrowth from the epidermis of true leaves, were ectopically developed on the surface of the *lec1* cotyledons (Meinke et al., 1994; West et al., 1994), indicating that heterochronic conversion was induced. Recent studies have revealed that LEC1 transcriptionally activates chloroplast biogenesis and photosynthesis in Arabidopsis (Pelletier et al., 2017; Jo et al., 2020), consistent with the observation that the *lec1* showed paler green coloration than wild-type (WT) embryos (Meinke, 1992; West et al., 1994). Intriguingly, LEC1 can also act as a pioneer TF to regulate flowering by reprogramming embryonic chromatin states (Tao et al., 2017).

Grass embryos are distinct from those of dicots and other monocots in many aspects (Armenta-Medina et al., 2021); for example, the grass embryo has a more complex structure. An embryonic envelope, consisting of the scutellum, coleoptile, coleorhiza, and epiblast (if it exists in the embryo of the species), is formed in grass to protect the plumule and radicle inside (Xu et al., 1999). Additionally, grass embryos can develop foliage leaves coupled with embryogenesis, indicating that early vegetative development is incorporated into the embryo development (Itoh et al., 2005). Moreover, cell division during Arabidopsis embryogenesis is stereotypical; however, for grass, such as rice and maize, there is no set pattern for the zygotic division after the first asymmetry division (Ishimoto et al., 2019).

According to morphological characteristics and landmark events, rice embryo development can

be divided into ten stages (Itoh et al., 2005). After fertilization (stage Em1), a globular embryo is developed around three days after fertilization (DAF) (Em2–Em4). The onset of coleoptile and the differentiation of the shoot apical meristem (SAM) and radical are then observed at 4 DAF (Em5). At 5–6 DAF, the first leaf is formed (Em6), and at 7–8 DAF, three foliage leaves are recognizable in the shoot apex (Em7). After that, there are no more morphological changes other than the remarkably enlarged embryo (Em8). Finally, the embryo gradually matures from 11 to 20 DAF (Em9) and acquires dormancy after then (Em10).

Hundreds of mutants showing abnormal embryo development have been isolated in rice (Hong et al., 1995; Nagato et al., 1989). In the past two decades, several key genes governing rice embryogenesis, embryo patterning, and organogenesis have been cloned, substantially expanding our understanding of the embryo development regulation in rice at a molecular level (Ishimoto et al., 2019; Yi et al., 2016; Sazuka et al., 2009; Nosaka et al., 2007; Hibara et al., 2009; Qi et al., 2020; Huang et al., 2017). However, ironically, several fundamental questions, such as identities and their homologies of the scutellum, coleoptile, coleorhiza, and epiblast, remained unanswered, although the debate has been provoked for centuries (Brown, 1960, 1965; Xu et al., 1999). Some mutants showing embryogenesis defects may provide novel perspectives for such questions. For example, the rice *shootless* (*shl*) mutants can develop scutellum but cannot form epiblast and coleoptile in the embryo, indicating that differentiation of the epiblast and coleoptile depends on the SAM, but that of the scutellum is regulated independently of SAM (Satoh et al., 1999). However, weak alleles of the *shl* mutants could form the SAM, but no coleoptile was produced (Satoh et al., 2003), suggesting that the coleoptile likely has a different identity to that of SAM-derived leaves. The unavailability of more informative mutants, such as *shl,* limits further discussions.

The angiosperm can be divided into chloroembryophytes and leucoembryophytes, depending on the presence and absence of chlorophyll (Chl) in embryos, respectively (Smolikova and Medvedev, 2016; Puthur et al., 2013). Some plant species, such as Arabidopsis, produce Chl when the embryo develops. As in leaves, Chl synthesized in the embryo also shows photosynthesis ability (Simkin et al., 2020). However, grass species, such as rice, cannot produce Chl when their embryos develop. To the best of our knowledge, what determines Chl

biosynthesis ability in plant embryos is completely unknown; however, several genes that contribute to Chl degradation for chloroembryos, whose mutation can lead to a stay-green phenotype of mature seeds, have been identified (Smolikova et al., 2017).

There are two LEC1-type genes, *OsNF-YB7* and *OsNF-YB9*, encoded by the rice genome (E et al., 2018). We previously found that *OsNF-YB7* or *OsNF-YB9* could recover the *LEC1* defects of the Arabidopsis mutant, *lec1-1* (Niu et al., 2021), indicating that the function of LEC1-type genes in rice and Arabidopsis is conserved. The LEC1-type genes, in Arabidopsis or rice, display a seed-preferential expression pattern. However, *OsNF-YB7* is predominately expressed in the embryo, while *OsNF-YB9* shows an endosperm-preferential expression (Niu et al., 2021). Given their distinct expression patterns in seeds, we assumed that *OsNF-YB7* and *OsNF-YB9* had been subfunctionalized during evolution. Null mutations of OsNF-YB9 resulted in reduced seed size and increased chalkiness of rice seeds but showed no effects on seed viability (Niu et al., 2021). However, *osnf-yb7* loss-of-function seeds cannot germinate using undetected mechanisms (Niu et al., 2021). This study found that *osnf-yb7* showed phenotypes similar to that of Arabidopsis *lec1*, such as dessication intolerance, reduced dormancy, and embryogenesis defects. Intriguingly, the coleoptile, epiblast, and coleorhiza were not observable in an *osnf-yb7* embryo, instead, a true leaf-like structure (LL) was developed from the scutellum. This allows us to discuss the homologies of complex embryo structures in grass; additionally, we found that *osnf-yb7* produced chloroembryos. As far as we know, this phenotype has never been reported in grass. Our findings suggested that OsNF-YB7 can repress the OsGLK1-mediated chlorophyll biosynthesis pathway in embryos, directly and indirectly.

Results

OsNF-YB7 is required for embryonic envelope development in rice

Previous studies have suggested that either knockout or knockdown of *OsNF-YB7* in rice is lethal (Niu et al., 2021; Ito et al., 2011; Zhang and Xue, 2013). To explore the cause of lethality, we analyzed embryo development in the *osnf-yb7* mutants that we previously generated (Niu et al., 2021). By confocal laser scanning microscopy (CLSM) observations, we found that there was no developmental difference between the mutant and WT embryos before 4 DAF (**Fig. 1A–F**). In the

5-DAF-old WT embryos, the coleoptile protruded from the ventral region above the SAM, which, nevertheless, was not observed in the mutant (**Figs. 1G and H**). Because *osnf-yb7-1* and *osnf-yb7-2*, two independent mull mutant lines, showed consistent phenotypes (**Fig. S1A–F**), we mainly used *osnf-yb7-1* for subsequent analyses. From a ventral side view of scanning electron microscopy (SEM), we found that the dome-like coleoptile of WT was surrounded by the scutellum at 5 DAF and protected by the ventral and lateral scales derived from the scutellum at 10 DAF (**Fig. 1I–L**). However, *osnf-yb7* embryos developed a flat leaf-like structure (LL) from the scutellum enclosing the shoot apex of mutant embryos (**Fig. 1M–P**). Investigation of the vertical and transverse sections further confirmed that the coleoptile was not developed, but replaced with a LL, in the *osnf-yb7* embryos (**Fig. 1Q–T**). Notably, the onset of LL in *osnf-yb7* coincided with coleoptile initiation in WT (**Figs. 1R and T**), indicating that LL is an analog or a heteromeric organ of the coleoptile. To unravel the LL's identity, we morphologically and histologically characterized it after germination (**Fig. 2A–L**). Hairs developed at the apical tip of LL, and trichomes were found on the LL's surface (**Figs. 2D, H and I**). The hair and trichomes do not develop on the WT coleoptile but can be found on the first leaf (**Fig. 2E–H**). These findings suggested that the LL resembles a leaf rather than a coleoptile. Additionally, the cell shape, cell composition, and cell arrangement of the LL were more similar to that of the first leaf of WT (**Figs. 2H and J**). Moreover, we found that there were multiple vascular bundles formed in the LL of *osnf-yb7*, whereas there were only two developed in a WT coleoptile (**Fig.2K and L**).

No epiblast and coleorhiza were formed in the embryos produced by *osnf-yb7* (**Fig. 1I–T**). The hypocotyl of *osnf-yb7* was strikingly longer than that of WT (**Figs. 1Q and S**). As indicated by the I_2-IK and coomassie brilliant blue staining assays, the scutellum of *osnf-yb7* accumulated significantly less starch grains and protein in the parenchyma cells (**Fig. S2A–D**). The WT scutellum differentiated a layer of palisade-shaped epithelial cells that could be observed in an 8-DAF-old embryo; however, the mutant scutellar epithelium was not strikingly different from the inner parenchyma cells regarding cell shape (**Fig. S2B and D**). It is worth noting that SAM establishment was not impaired in *osnf-yb7*, given that the onset of leaf primordium was normal in 5-DAF-old embryos (**Figs. S2E and F**). These findings suggested that *OsNF-YB7* is indispensable for embryogenesis in rice.

Transcription disorders in the *osnf-yb7* embryos

We next performed RNA-seq analysis to investigate the transcriptomic changes in 5- and 10-DAF-old embryos of *osnf-yb7*. There were 1,311 and 3,006 genes down- and upregulated in the 5-DAF-old embryos of *osnf-yb7*, respectively, compared with the WT embryos at the same age, using the threshold fold change > 2 and Bonferroni $p < 0.05$ (**Table S1**). Similarly, 1,280 and 4,100 genes were down- and upregulated, respectively, in the *osnf-yb7* embryos at 10 DAF (**Table S2**). However, most of the differentially expressed genes (DEGs) identified at 5 and 10 DAF were common (**Fig. 3A**). Notably, the number of upregulated genes was consistently higher than that of downregulated ones, indicating that OsNF-YB7 mainly functions as a transcriptional repressor in rice embryos. Interestingly, we found that the most upregulated genes at 10 DAF, whose fold changes ranked the top 100 in *osnf-yb7*, are usually highly expressed in vegetative tissues but showed less expression in the embryo (**Fig. 3B**). Instead, the most downregulated genes (top 100) display an overall embryo or caryopsis preferential pattern (**Fig. 3B**). This provides transcriptional evidence for the assumption that the LL of *osnf-yb7* is more like a vegetative (i.e., leaf) than an embryonic structure.

Itoh *et al.* (2016) identified a set of genes showing tissue-specific upregulation in the shoot, scutellum, root, or epiblast/coleorhiza in the embryo. We found that approximately 40% of these genes displayed differential expression in the *osnf-yb7* embryonic tissues (**Table S3**), suggesting that the *OsNF-YB7* defects resulted in extensive deregulation of embryogenesis. In a genome-wide analysis, approximately 30% and 23% of the DEGs we identified in 5- and 10-DAF-old mutant embryos, respectively, were downregulated (**Fig. 3A**). However, for the scutellum, preferential genes more than 52% and 42% DEGs were downregulated at 5 and 10 DAF (**Figs. 3C and D**), respectively, indicating that the downregulated genes were over-represented in the scutellum of *osnf-yb7*. In contrast, only a small portion of the epiblast (9%–16%) and root preferential DEGs (13%–16%) were downregulated (**Fig. 3C and D**). The results implied that the scutellum showed unique expressional changes in *osnf-yb7*, in line with *OsNF-YB7* is a scutellum-preferential gene (Niu et al., 2021; Zhang and Xue, 2013).

TFs play vital roles in embryogenesis (Itoh et al., 2016). Among the 1,877 rice TFs deposited in

PlantTFDB, 359 and 389 showed differential expression in 5- and 10-DAF-old *osnf-yb7* embryos, respectively, compared with the WT (**Table S4**). Distinct TF families were enriched in the upregulated and downregulated TFs. For example, AP2, B3, NF-YA, ARF, and GRF family TFs were over-represented in the downregulated DEGs; whereas, AUX/IAA and RAV TF family members were over-represented in the upregulated DEGs that were identified from the *osnf-yb7-1* embryos (**Fig. 3E and F**). Notably, many differentially expressed TFs encode homeobox members that play essential roles in embryogenesis and embryo patterning (**Table S4**). For example, the ZF-HD subfamily genes were enriched in the downregulated DEGs at 5 and 10 DAF (**Fig. 3E and F**). A group of WOX genes was also suppressed in the mutant, although only enriched at 5 DAF (**Fig. 3E**). In contrast, HD-ZP subfamily TFs were over-represented in the upregulated DEGs at 5 and 10 DAF (**Fig. 3E and F**). Likewise, many three-amino-acid-loop-extension classes of homeobox genes, including the KNOTTED-like (KNOX) homeodomain and BEL1-like (BELL) homeodomain members, were activated in the 10-DAF-old *osnf-yb7-1* embryo (**Fig. 3F**).

The embryo of *osnf-yb7* remains active after embryogenesis

For WT, there were 3,266 and 1,193 genes down- and upregulated in the embryos at 10 DAF compared with the mRNA profiles of 5-DAF-old embryos (**Fig. 3A, Table S5**). However, for *osnf-yb7*, the number of down- and upregulated genes identified between 5- and 10-DAF-old mutant embryos were 1,553 and 999, respectively (**Fig. 3A, Table S6**). The results suggested that more genes were transcriptionally repressed at 10 DAF in WT than in *osnf-yb7*. Because these DEGs reflected transcriptional changes in different developmental stages (10 DAF *vs.* 5 DAF), we termed them development-related DEGs (drDEGs). Intriguingly, Gene Ontology (GO) analyses showed that distinct biological processes were enriched for the WT and *osnf-yb7* drDEGs (**Fig. 3G**). For example, the terms “response to stimulus” and “stress response” were enriched for the upregulated drDEGs in WT, which is expected due to dehydration onset in embryos at 10 DAF. However, the same terms were enriched for the downregulated-, but not for the upregulated drDEGs, identified in *osnf-yb7* (**Fig. 3G**). Genes involving expression and translation were over-represented for the upregulated drDEGs in *osnf-yb7*, and the downregulated drDEGs in WT (**Fig. 3G**). Moreover, several terms associated with active cell activities, such as “signal transduction” and “cell cycle,” were specifically enriched for the upregulated drDEGs in *osnf-yb7*

(**Fig. 3G**). The transcriptional differences suggested that *osnf-yb7* embryos were more active than WT at 10 DAF. Consistent with this, a 2,3,5-triphenyltetrazolium chloride (TTC) staining assay showed that staining reactions in the shoot and root of the WT 10-DAF-old embryos were not as active as that reacted in the mutant, indicating the *osnf-yb7* embryos were metabolically overactivated (**Fig. 3H and I**). After finishing embryogenesis, there was no morphological change in a WT rice embryo (Itoh et al., 2005). However, because the developmental cessation was largely lost in *osnf-yb7*, many morphological variations could be observed for the mutant embryos at □15 DAF (**Fig. 3J and K**).

Loss-of-function of *OsNF-YB7* weakens dormancy

Persistent growth of the *osnf-yb7* embryos indicates that dormancy was a breakdown in the mutants. Consistent with this, several key genes involving rice dormancy, such as *OsVP1*/*OsABI3* (Wang et al., 2020; Sugimoto et al., 2010; Chen et al., 2021), *OsFLF1*, and *OsGD1* (Guo et al., 2013), are significantly suppressed in the mutant (**Fig. S3A–C**). However, we found that many genes governing ABA biosynthesis were overall activated in the mutant (**Fig. 4A and B**), which is possibly feedback to the decreased ABA content in *osnf-yb7* (**Fig. 4C**). Furthermore, some ABA-responsive genes, including *OsVP1*/*OsABI3*, *OsABI4*/*OsERF117*, and *OsABI5*/*OsZIP10*, and their downstream genes, such as *Sdr4*, were significantly suppressed in the *osnf-yb7* embryos,at either 5 or 10 DAF (**Fig. 4 B**). However, we found that some key components involving stress-induced ABA signaling were activated, rather than inactivated, in *osnf-yb7*. For example, *OSBZ8/OsbZIP05*, *OsABIL1,2,3*, *OsABF1/OsbZIP12*, and *OsABF2/OsbZIP46* showed significantly higher expression in the mutant at 10 DAF (**Fig. S3D–F, Table S7**). These findings strongly indicated that OsNF-YB7 selectively repressed dormancy-related ABA signaling genes, such as *OsVP1/OsABI3, OsABI4/OsERF117*, and *OsABI5/OsZIP10*, in the embryo.

GA acts as an intrinsic signal to break dormancy; *OsGA20ox1* and *OsGA3ox2*, two important GA biosynthetic genes were significantly upregulated in *osnf-yb7* (**Fig. 4B, Figs. S4A and B, and Table S8**). In line with this, GA_1 and GA_4, two active GA molecules in rice, were highly accumulated in the *osnf-yb7* embryo at 10 DAF (**Fig. 4D and E**). The ratio, ABA:GA, which is important for maintaining seed dormancy, was substantially decreased in the mutant (**Fig. 4F**) due to the

decreased ABA and increased GA content in the mutant. Previous studies showed that the germination of seeds is associated with the activation of RAmy1A, an α-amylase glycoprotein induced by the GA-induced GAMYB in rice (Morita et al., 1998). *GAMYB* was significantly activated in the mutant embryos, and accordingly, *RAmy1A* was highly expressed in *osnf-yb7-1*, whereas there was no *RAmy1A* transcript detectable in the WT embryo at 10 DAF (**Fig. S4C and Table S8**). Altogether, we assumed that the breakdown of *osnf-yb7* dormancy was caused by activating GA biosynthesis, coupled with the repression of the ABA-induced dormancy signals.

OsNF-YB7 is essential for the acquisition of desiccation tolerance

Although *osnf-yb7* embryo is more active after embryogenesis (**Fig. 3G–K**), the TTC staining analysis showed that mature seeds of *osnf-yb7* were less vigorous than the WT after imbibition for 12 h (**Fig. 4G and H**). Therefore, most of the dehydrated *osnf-yb7* seeds are not germinable (Niu et al., 2021). However, we found that if the seeds were not desiccated, *osnf-yb7* could germinate. Furthermore, using the seeds harvested before drying (□25 DAF), *osnf-yb7* germinated much faster than WT seeds (**Fig. 4I**). However, the subsequent seedling development of *osnf-yb7* was arrested (**Fig. 4J**).

The findings suggested that *OsNF-YB7* is required for the acquisition of desiccation tolerance in rice. In favor of this, the genes encoding late embryogenesis abundant (LEA) proteins that accumulate during late stages of embryogenesis and associate with dehydration were significantly repressed in the 10-DAF-old mutant embryo. However, there was no expression difference of these genes between the WT and *osnf-yb7* embryos at 5 DAF (**Fig. S5A**). Among these LEA-encoding genes, *OSEM*, *Rab16A,* and *REG2* are marker genes activated at the Em8 phase (Itoh et al., 2005). However, their expressions were largely repressed in *osnf-yb7* embryos at 10 DAF (**Fig. S5B–D**).

OsNF-YB7 represses chlorophyll biogenesis and photosynthesis in the embryo

The embryos produced by *osnf-yb7* embryos were greenish owing to the activation of Chl biogenesis (**Fig. 5A–D**). Intriguingly, the quantification analysis showed that the content of Chlb was not strikingly different between *osnf-b7* and WT, but the mutant embryos accumulated

more Chla, at either □15 DAF or maturation stage (**Fig. 5C and D**). Furthermore, chlorophyll autofluorescence could be observed in an *osnf-yb7* embryo at as early as 5 DAF (**Fig. S6A and B**). Additionally, many genes responsible for rice chlorophyll biogenesis were activated in the mutant embryos at either 5- or 10 DAF (**Fig. S6E and F**). In consequence, as revealed by the Mapman analysis, genes involving photosynthesis were dramatically enriched for DEGs, and the vast majority of the genes was upregulated (**Fig. S7A–D**).

Several TFs have been identified in plants for regulating chlorophyll biogenesis or chloroplast development (Jarvis and López-Juez, 2013). Some TFs, such as rice *GOLDEN 2-like1* (*OsGLK1*), *HY5-like1* (*OsHY5L1*), *PIF-like14* (*OsPIL14*), and rice *GATA Nitrate-inducible Carbon-metabolism-involved* (*OsGNC*), were significantly upregulated in the *osnf-yb7* embryos; among which, *OsGLK1* was the most activated gene (**Fig. 5E–H**). Overexpression of *OsGLK1* can significantly increase chlorophyll content in rice (Nakamura et al., 2009). By surveying the genes upregulated in an *OsGLK1* overexpression line (Nakamura et al., 2009), we found that most of the *OsGLK1* activated genes (□70.2%) were also upregulated in the *osnf-yb7* embryos at either 5- or 10-DAF (**Fig. 5I**). To explore the possibility that OsNF-YB7 directly represses the expression of *OsGLK1*, we conducted a dual-luciferase (LUC) assay to test the hypothesis. The results showed that OsNF-YB7 significantly repressed the activities of the LUC reporter driven by the *OsGLK1* promoter (**Fig. 5J and K**).

Meanwhile, we examined the interaction between OsNF-YB7 and OsGLK using yeast two-hybrid assays (Y2H). We fused full-length OsGLK1 with the GAL4 DNA-activation domain and full-length OsNF-YB7 with the GAL4 DNA-binding domain. The results showed that OsNF-YB7 interacts with OsGLK1 in yeast (**Fig. 6A**). The proteins also showed strong interactions in the epidermal cells of tobacco, as indicated by the split complementary LUC assay (**Fig. 6B**). The bimolecular fluorescent complementary (BiFC) analysis suggested that the interaction occurred exclusively in the nuclei (**Fig. 6C**). Moreover, we transiently coexpressed OsNF-YB7 that tagged with green fluorescent protein (YB7-GFP), and OsGLK1 that tagged with 3x flag (GLK1-flag) in rice protoplast. Also, the co-immunoprecipitation (CoIP) analysis showed that GLK1-flag could be co-immunoprecipitated in rice using the anti-GFP antibody (**Fig. 6D**). Collectively, these findings suggest that OsNF-YB7 interacts with OsGLK1 both *in vivo* and *in vitro*.

The primary target genes of GLK1 in Arabidopsis are light-harvesting and Chl biosynthesis-related genes (Nagatoshi et al., 2016). For example, the genes encoding protochlorophyllide oxidoreductase (POR), which catalyzes the reactions of protochlorophyllide (Pchlide) to chlorophyllide for Chl synthesis, were transcriptionally activated by *GLK1* in Arabidopsis (Waters et al., 2009). Therefore, *OsPORA* and *LHCB4* (*Light-Harvesting Complex B4*), a Chla-b binding protein-encoding gene that activated by OsGLK1 in rice (Zhang et al., 2021), were selected to analyze whether OsNF-YB7 disturbs the OsGLK1-mediated chlorophyll biosynthesis, given their expression was substantially activated in the *osnf-yb7* embryos (**Fig. 6E and F**). As expected, the transient expression of OsGLK1 in rice protoplast substantially activated the reporter gene driven by the promoters of *OsPORA* and *LHCB4*, indicating that these genes are transcriptionally targeted by OsGLK1 (**Fig. 6H–I**). When we coexpressed OsNF-YB7 with OsGLK1, the activation ability of OsGLK1 was significantly repressed (**Fig. 6H–I**). However, OsNF-YB7 alone did not show influences on the expression of the reporter (**Fig. 6H–I**). Altogether, we assumed that OsNF-YB7/OsGLK1 dimerization reduces the ability of OsGLK1 for Chl biogenesis.

Collectively, our results suggest that the activation of OsGLK1, at either transcriptional or post-translational level, contributes to Chl accumulation in the *osnf-yb7* embryos. To test this, we generated high-order mutants of *OsNF-YB7*, *OsGLK1,* and *OsGLK2*, considering there are redundancies between *OsGLK1* and *OsGLK2* (Sakuraba et al., 2017; Wang et al., 2013). Using the CRISPR/Cas9 cassette that included three tandemly arrayed guide RNAs targeting *OsNF-YB7*, *OsGLK1,* and *OsGLK2*, respectively, we successfully obtained the *osnf-yb7*;*osglk2* double mutant and the *osnf-yb7*;*osglk1*;*osglk2* triple mutant at the T_0 generation (**Fig. S8**). By analyzing embryos the mutants produced, we found that *osnf-yb7*;*osglk2* and *osnf-yb7*;*osglk1*;*osglk2* displayed embryo morphology similar to that of *osnf-yb7* (**Fig. 6J–M**). However, the Chl accumulated in *osnf-yb7*;*osglk1*;*osglk2* was less than in *osnf-yb7* and *osnf-yb7*;*osglk2* (**Fig. 6J–M**). In comparison to the achlorophyllous embryo of WT, the *osnf-yb7*;*osglk1*;*osglk2* triple mutant still showed somewhat green coloration in apical part of the embryos (**Fig. 6M**), suggesting that in addition to *OsGLKs*, there are some other players contribute to the Chl biogenesis in the embryos of *osnf-yb7*.

Functional conservation of *ZmLEC1* genes for embryo development in maize

There are three LEC1-type genes encoded by the maize genome, among which, Zm00001d051697 and Zm00001d017898 are phylogenetically closer to OsNF-YB7, while Zm00001d045772 is a homolog of rice OsNF-YB9 (**Fig. 7A**). Similar to their rice homologs, Zm00001d051697 and Zm00001d017898 are predominantly expressed in the embryo, whereas Zm00001d045772 is endosperm preferentially expressed in our previous report (E et al., 2018). To detect whether Zm00001d051697 and Zm00001d017898 play a conserved role in embryo development, we generated double mutants of the genes using a CRIPSR/Cas9 gene-editing approach. Because of high similarities between Zm00001d051697 and Zm00001d017898, we could use the same guard RNA to knock out the two genes simultaneously (**Fig. S9A**). To increase the chance to obtain double mutants, we designed two targets for gene editing. We obtained five independent transgenic events, two of which produced seeds showing similar phenotypes to that of the *osnf-yb7* mutants. By sequencing the T_2 individuals showing a phenotype, we found that both Zm00001d051697 and Zm00001d017898 were mutated, while the ones with only one gene-edited showed normal development (**Fig. S9B**).

All seeds produced by line A05-01-1 exhibited embryo defects. We, therefore, used this line for subsequent phenotypic analyses. Like that of *osnf-yb7*, post-germination development of A05-1-1 was arrested (**Fig. 7B**). No coleoptile was developed in the mature maize mutant seeds; instead, we could observe a LL structure after imbibition (**Fig. 7C–H**). The maize embryo does not have an epiblast, but we could still find that the structure surrounding the plumule-radicle axis at the ventral side was not developed in the *lec1* mutant (**Fig. 7C, D, G, and H**), resembling the observation that epiblast was disappeared in the *osnf-yb7* embryos. Similarly, the coleorhiza of the *lec1* mutant in maize was also mal-developed (**Fig. 7C and D**). However, some of the dried mutant seeds were germinable and can develop into a fertile plant (**Fig. S9C**). A close observation of the germinated *lec1* maize seeds suggested that a LL structure replaced the coleoptile, leaving the inside leaves unprotected (**Fig. 7I–L**). The cross-sections of germinated maize embryos showed that the LL structure of the *lec1* mutant is a scutellum derivative (**Fig. 7K and L**), consistent with the phenotype that showed in the rice mutant. Notably, the maize *lec1* embryos were achlorophyllous (**Fig. 7C–H**). This was possible because multiple layers of bracts inhibited light from penetrating the ear. In favor of this hypothesis, blocking light perception by covering

aluminum foils on a rice panicle resulted in achlorophyllous embryos of *osnf-yb7* (**Fig. S10**). Altogether, phenotypical similarities between the rice and maize *lec1* mutants strongly suggested that the LEC1-type genes are functionally conserved for grass embryo development.

Discussion

LEC1-type genes play a conserved role in plant seed development

LEC1-type genes originated from non-LEC1 type NF-YB genes in basal land plants (Xie et al., 2008; Cagliari et al., 2014) and possibly played a crucial role in the evolution of seed in plants (Jo et al., 2019). The LEC1-type genes in grass species have been divergent into two subgroups: OsNF-YB7-like and OsNF-YB9-like (E et al., 2018). OsNF-YB7-like genes are phylogenetically closer to LEC1 and L1L of Arabidopsis, whereas the OsNF-YB9 homologs are found only in grass, indicating that OsNF-YB9 was evolved after the divergence of grass. *LEC1* is expressed in the embryo and endosperm soon after fertilization in Arabidopsis (Xie et al., 2021). *OsNF-YB7* exclusively expresses in the embryo, while the *OsNF-YB9* are endosperm preferentially expressed in rice (Niu et al., 2021). Differentiated expression patterns of the OsNF-YB7-like and OsNF-YB9-like genes were also found in maize, sorghum, and barley (E et al., 2018). These different expression patterns suggest subfunctionalization of the LEC1-type genes in grass. A recent study showed that the endosperm-expressed *LEC1* in Arabidopsis is sufficient for embryo maturation (Xie et al., 2021). In the case of rice, *osnf-yb9* showed no embryo defects (Niu et al., 2021); as well, *osnf-yb7* showed no endosperm phenotype (**Fig. S1A and Fig. S11A**). Moreover, by investigating the expression profiles in the *osnf-yb7* endosperm at 10 DAF, we found that only a small number of genes showed differential expression (88 downregulated and 136 upregulated) in comparison to the WT, further confirming that *OsNF-YB7* and *OsNF-YB9* are confined to different compartments (i.e., embryo and endosperm, respectively) for function (**Fig. S11B and Table S9**). However, we did find expression changes of some genes. For example, *OsNF-YB9* was significantly activated in the *osnf-yb7* endosperm, while several genes in response to auxin were downregulated (**Fig. S11C**).

We previously reported that *OsNF-YB7* and *OsNF-YB9* could complement the *lec1* defects in Arabidopsis (Niu et al., 2021). Here we found that almost all developmental defects showed in

lec1 could be observed in *osnf-yb7*, including loss of quiescence, weakened dormancy, and desiccation intolerance (**Figs. 3 and 4**). Embryogenesis defects of *lec1* and *osnf-yb7* were also comparable. Both LEC1-type mutants showed over-proliferation of suspensors; the hypocotyl of the mutants was not as bent as the WT (**Fig. 1I–T**). A heterochronic conversion was induced in *lec1*, for whose cotyledons acquired characteristics displayed in a true leaf (Meinke et al., 1994; West et al., 1994). Likewise, an LL was derived from the *osnf-yb7* scutellum at the corresponding regions where WT's coleoptile and epiblast originated. Therefore, we believed that the LL of *osnf-yb7* is not a coleoptile analog, but more like a true leaf in several aspects (**Fig. 2A–L**): (1) trichomes were developed at the tip and on the surface of the LL structure; (2) cell arrangement of the LL structure was different from that of the coleoptile; (3) multiple vascular bundles were developed rather than two. This evidence suggested a leaf identity of LL. Additionally, the maize *lec1* mutants, we generated also displayed similar embryo morphology: the coleoptile was substituted by a structure similar to foliage (**Fig. 7B–L**).

Reconsideration of the homologies of complex embryo structures in grass

Several distinct concepts have been proposed to interpret what the grass embryonic structures represent. The scutellum is considered equivalent to the cotyledon, either entire or partial of it (Brown, 1965, 1960; Xu et al., 1999; Chandler, 2008; Satoh et al., 1999). However, no agreements have been achieved regarding the homologies of the epiblast and coleorhiza, which have been debated for centuries (see reviews Brown, 1965, 1960). The homology of coleoptile is a more controversial topic. The grass coleoptile has been proposed as a part of the cotyledon, a leaf (first, second, or third leaf), a leaf sheath, or an innovation of grass that does not have a counterpart in the dicot embryo (see reviews Brown, 1965, 1960).

The coleoptile primordium was formed from the ventral side of the scutellum; the epiblast and coleorhiza, and the lateral and ventral scales that are covering the coleoptile, are directly derived from the scutellum, and there was no primordium differentiated for forming these structures (Xu et al., 1999; Itoh et al., 2005; Brown, 1960, 1965). Mutants that showed specific embryo defects, such as *osnf-yb7,* may provide new insights for the debating. The entire embryonic envelope development was impaired in *osnf-yb7*: coleoptile, coleorhiza, and epiblast were completely lost

(**Fig. 1I–T**); the scutellum accumulated less storage reserves, and the palisade-shaped epithelial cells were not differentiated (**Fig. S2A–D**). A LL structure (with somewhat foliage identities) was developed from where the coleoptile and epiblast originated. *LEC1* defects resulted in a heterochronic conversion for the Arabidopsis cotyledons. Given the parallel phenotypes of *lec1* and *osnf-yb7*, we inferred that the structures of WT that transformed into the LL structure in *osnf-yb7* are equivalent to the cotyledons in Arabidopsis (**Fig. S12 A–C**). For this consideration, the coleoptile and epiblast are most likely the cotyledon analogs in rice. The epiblast is an extension of the coleorhiza (Brown, 1960, 1965) and the midrib of the LL structure is extended from the main scutella vascular bundle (**Fig. 1Q–T**). Considering these, we propose a hypothesis that the entire embryonic envelope is the cotyledon of grass (**Fig. S12 A–C**). The expression profiles of the laser-microdissected rice embryo tissues favor the idea that the embryonic envelope is a continuum sharing similar gene expression. By reanalyzing the data generated by Sato *et al*. (2016), we found that mRNA profiles of the scutellum and epiblast/coleorhiza were similar but distinct from those of the shoot and root (**Fig. S13**).

The role of the LEC1-type genes in plant chlorophyll biogenesis

Plants, such as Arabidopsis bear chlorophyllous embryos. Chl can be detected as early as the globular stage in Arabidopsis, and the embryo turns green toward the end of the late-heart stage (Parcy et al., 1997). However, mature embryos are de-greened because Chl degradation couples with seed maturation (Smolikova et al., 2017). Previous studies showed that the mature embryos of *lec1* were paler than the WT (Meinke, 1992; West et al., 1994), indicating that LEC1 acts as a positive regulator for Chl biogenesis. In agreement, comprehensive transcriptome analyses showed that LEC1 could transcriptionally activate dozens of chloroplast biogenesis and photosynthesis-related genes in Arabidopsis and soybean embryos (Pelletier et al., 2017; Jo et al., 2020). Like many other grass species, the embryos of rice are achlorophyllous. This study found that, in contrast to Arabidopsis, null mutation of *OsNF-YB7* activated photosynthesis and Chl biosynthesis in rice. Consequently, green embryos with significant quantities of Chl were produced by the *osnf-yb7* mutants (**Figs. 5A–D and S6A and B**). These findings indicated that the LEC1-type gene likely acts as a negative regulator in rice, but a positive regulator in Arabidopsis, for Chl biosynthesis.

By surveying the literature, we noticed that Meinke (1992) reported that the cotyledons of *lec1* mutant remained green unusually late in development. Although there was no significant Chl content difference when using whole seeds for quantification, Parcy *et al*. (1997) did observe that the tip of *lec1* cotyledons accumulates more Chl. Moreover, the *lec1;abi3* double mutant embryos produced a much higher Chl than the *abi3* single mutant (Parcy et al., 1997). These findings challenge the concept that LEC1 positively regulates Chl biosynthesis and photosynthesis in Arabidopsis. It is worth noting that in the *osnf-yb7* embryos, Chl also preferentially accumulated in the tip-end of the LL structure (**Fig. S6A and B**). Therefore, LEC1 may play a role in Chl biogenesis in different parts of the Arabidopsis cotyledons. Moreover, most studies on Arabidopsis emphasize *LEC1*'s importance in embryo development at the maturation stage. Indeed, by comparing the transcriptomes of WT and *lec1* seeds, the major difference in mRNA profiles is observed at maturation (Pelletier et al., 2017). However, *LEC1* is activated within 24 h after fertilization (Lotan et al., 1998), its role in the early embryo developmental stages for Chl biogenesis is still unknown.

Photosynthesis and Chl biogenesis-related genes were enriched for the LEC1 binding targets (Pelletier et al., 2017), many of which were also differentially expressed in *osnf-yb7*, indicating that they are likely common downstream targets of the LEC1-type TFs in plants. Interestingly, we found that *OsGLK1*, *OsPIL14*, *OsHY5L,* and *OsGNC* were upregulated in the *osnf-yb7* embryos (**Fig. 5E–H**). These TFs are important for chloroplast development and photomorphogenesis in rice (Nakamura et al., 2009; Li et al., 2019; Bai et al., 2019). The reporter gene driven by the *OsGLK1* promoter was transcriptionally inactivated by OsNF-YB7 (**Fig. 5J and K**), further indicating that *OsGLK1* could be a direct downstream target of OsNF-YB7. Previous studies have shown that LEC1 could interact with different TFs for function (Huang et al., 2015b; Boulard et al., 2017; Huang et al., 2015a; Hu et al., 2018). For example, LEC1 binds to TRICHOMELESS2 (TCL2) to repress the expression of genes involving trichome development during embryogenesis (Huang et al., 2015a). Here, we found that OsNF-YB7 interacted with OsGLK1 *in vitro* and *in vivo* (**Fig. 6A–D**). OsGLK1 activated the expression of *OsPORA* and *LHCB4*, whereas OsNF-YB7 alone showed no impact on these genes (**Fig. 6G–I**). However, Coexpression of OsGLK1 and OsNF-YB7 in protoplasts repressed the ability of OsGLK1 to activate *OsPORA* and *LHCB4* (**Fig. 6G–I**). Most of

463 the OsGLK1-induced genes were also activated in *osnf-yb7* (**Fig. 5I**). Therefore, we believe that
464 OsNF-YB7 plays a dual role in regulating Chl biosynthesis and photosynthesis in rice embryos
465 (**Figs. S14A and B**). First, it represses the downstream genes achieving by its function as a
466 transcriptional inactivator; second, OsNF-YB7 can interact with TFs such as OsGLK1 to disturb
467 their activation abilities for Chl biosynthesis and photosynthesis-related genes (**Figs. S14A and B**).
468 Intriguingly, a previous study showed that OsNF-YB2 positively regulates chloroplast
469 development in rice (Miyoshi et al., 2003), which suggests that the LEC1-type and non-LEC1-type
470 NF-Y members can play a distinct role in Chl biogenesis.

471 ***OsNF-YB7* and somatic embryogenesis**

472 *LEC1* is essential for inducing somatic embryogenesis in Arabidopsis. Ectopic expression of *LEC1*
473 can induce the expression of embryo-specific genes in vegetative cells and initiate the formation
474 of somatic embryos (Lotan et al., 1998). In contrast, the ability to form somatic embryos was
475 significantly reduced for the *lec1* mutant (Gaj et al., 2005). Notably, homozygous mutants of
476 *osnf-yb7* that regenerated from the calli were obtainable at T_0 generation. This indicated that a
477 de-differentiated totipotent cell carrying non-functional LEC1 alleles could still develop into a
478 somatic embryo and be further regenerated into a viable and fertile plant. In this scenario, *LEC1*
479 is not indispensable for rice somatic embryogenesis. However, the *LEC1* defects of the
480 regenerated *osnf-yb7* plant could not be transmitted to the offspring due to zygotic
481 embryogenesis defects shown in this study, even using embryo rescue technology. This suggests
482 that *OsNF-YB7* plays a different role in zygotic and somatic embryogenesis, which deserves
483 further investigation.

484 **Materials and Methods**

485 **Plant growth conditions**

486 The rice plants were grown in the experimental field of Yangzhou University in Yangzhou, Jiangsu
487 Province, and in Lingshui, Hainan Province, China, with regular water and nutrient management.
488 The spikelets were marked on the day of anthesis for sampling different aged embryos and
489 endosperm. The maize used in this study was grown in the experimental field of Biogle GeneTech

in Xishuangbanna, Yunnan Province, China. Because the seeds produced by *osnf-yb7* were inviable, the mutants used were propagated asexually by ratooning as described previously (Cheng et al., 2020). The rice and maize seeds were germinated in a growth chamber. The chamber temperature was maintained at 28°C with 12 h/12 h light/dark cycle.

Generation of CRISPR/Cas9 mutants

The *osnf-yb7* mutant lines used in the study were previously generated in our lab (Niu et al., 2021). The higher-order mutants of *OsNF-YB7 OsGLK1* and *OsGLK2* mutants were generated using a previously described method for multiple gene editing (Cheng et al., 2020) in Zhonghua11 (*O. sativa* ssp. *japonica*). The maize *lec1* mutant lines were generated by Weimibio Co. in the genetic background of KN5585. Approximately 300 bp genomic segments harboring each CRISPR targeting site was amplified by PCR and subjected to Sanger sequencing for genotyping to screen the mutants. The primers used for mutant generation and for genotyping are listed in **Table S10.**

Sectioning, staining, and microscopic observation

For semithin section preparations, different aged embryos of WT and *osnf-yb7* were dissected under a dissecting microscope and were then fixed in FAA solution (60% (v/v) ethanol, 5% (v/v) glacial acetic acid, and 5% (v/v) formaldehyde) and subjected to vacuum pumping for 40 min. After dehydration through an ethanol series and infiltrated with xylene for embedding in resin, the embedded samples were sectioned at 2.5 μm thickness using a rotary microtome (Leica). Sections were then stained with 0.1% toluidine blue, coomassie brilliant blue, or I_2-KI solution (80-mg KI, 10-mg I2 per ml) and photographed using an Olympus IX71 microscope.

The glumes were removed from rice seeds for free-hand sectioning, and then the caryopsis was carefully cut with a double-edged blade. For desiccated mature seeds, the caryopses were soaked in water at 4°C overnight before the experiment. The sections were then photographed or stained with TCC solution (Solarbio) according to the manufacture's protocol.

CLSM was performed as described previously (Cheng et al., 2020). Images of the PI-stained embryos were taken using an LSM710 (Zeiss) microscope with excitation/emission wavelengths

of 559/619 nm.

For SEM analysis, the rice embryos were fixed overnight at 4°C in 2.5% glutaraldehyde in phosphate buffer (0.1 M, pH 7.0), washed three times in the phosphate buffer (0.1 M, pH 7.0) for 15 min at each step, then, postfixed with 1% OsO4 in phosphate buffer for 2 h and washed three times in phosphate buffer. The samples were dehydrated through an ethanol series, then transferred to absolute ethanol. The dehydrated sample was coated with gold-palladium using an ion sputterer (EM SCD500, Leica) and imaged using a SEM (GeminiSEM 300, Zeiss).

RNA extraction and real-time PCR assay

Total RNA was isolated using the RNA-easy Isolation Reagent (Vazyme, R701-01). One microgram of total RNA was used for cDNA synthesis with the First Strand cDNA Synthesis kit (Vazyme, R123-01). Real-time RT-PCR was performed using the SYBR qPCR Master Mix (Vazyme, Q111-02) in the CFX Connect Real-Time PCR Detection platform (Bio-Rad). The experiments were performed using at least three biological replicates. The relative expression level of the tested genes was normalized to the rice Ubiquitin gene (GenBank accession AF184280) and calculated using the $2^{\Delta Ct}$ method. The primers used for qRT-PCR were listed in **Table S10**.

RNA-seq and differential expression analysis

Total RNA was extracted from the 5- and 10 DAF embryos and 10 DAF endosperm of the WT and *osnf-yb7*. Three biological replicates for each sample were set. The qualified samples were submitted to BGI for library preparation and sequencing. The CLC Genomics Workbench 12.0 software was used for RNA-seq data analysis. The thresholds fold change > 2 and Bonferroni $p < 0.05$ were used for defining a DEG. The software MapMAN was used for MapMAN pathway analysis (Usadel et al., 2009). The online tool AgriGO 2.0 was used for GO analysis (Du et al., 2010). TBtools was used for heatmap generation (Chen et al., 2020).

Hormone extraction and quantification

First, approximately 0.1-g embryo was collected from the WT and *osnf-yb7* for hormone extraction and quantification. Then, the contents of IAA, ABA, $GA_{1,}$ and GA_4 were measured by

high-performance liquid chromatography–tandem mass spectrometry (Agilent, 1290) according to the previously described procedures (Cheng et al., 2020).

Yeast two-hybrid assays

The coding sequences (CDS) of *OsGLK1* and *OsNF-YB7* were cloned into the pGADT7 and pGBKT7, respectively. The constructs were cotransformed into yeast strain AH109 using Frozen-EZ Yeast Transformation II kit according to the manufacturer's protocol. The empty pGADT7 and pGBKT7 vectors were cotransformed in parallel as negative controls. The transformants were first selected on synthetic dropout medium (SD/-Trp-Leu) plates. Then, we tested protein-protein interactions using selective SD/-Trp-Leu-His and SD/-Trp-Leu-His-Ade dropout medium. Interactions were observed after 3 d of incubation at 28°C. The primers used for generating these constructs are listed in **Table S10**.

Split complementary LUC assays

Split complementary LUC assays were performed as previously described (Niu et al., 2020). The CDS of *OsGLK1* and *OsNF-YB7* was cloned into JW771 and JW772 vectors to generate nLUC-OsGLK and cLUC-OsNF-YB7, respectively. The constructs were introduced into Agrobacterium tumefaciens strain GV3101 and then co-infiltrated into *N. benthamiana* leaves, and the LUC activities were analyzed after 48-h infiltration using Tanon Imaging System (5200 Multi; Tanon). The primers used for vector construction are shown in **Table S10**.

Bimolecular fluorescence complementary assays

The CDS of *OsGLK1* and *OsNF-YB7* was cloned into the pSPYNE (nYFP) and PSPYCE (cYFP). The prepared plasmids were transformed into Agrobacterium strain GV3101, and the indicated transformant pairs were infiltrated into *N. benthamiana* leaves. After 48 h after infiltration, the fluorescence signal of yellow fluorescent protein (YFP) was observed with confocal microscopy (Carl Zeiss, LSM 710). Images were captured at 514 nm laser excitation and 519–620 nm emission for YFP. The primers used for vector construction are shown in **Table S10**.

Co-Immunoprecipitation Assays

Co-immunoprecipitation assays were performed in the Rice protoplast system as described (Zhang et al., 2011). The CDS of *OsGLK1* and *OsNF-YB7* was cloned into pUC19-35S-FLAG-RBS vector and pJIT163-GFP driven by 35S promoter, respectively. Ten micrograms of plasmid DNA (OsGLK-GFP, GFP, and OsNF-YB7-Flag) was transformed or cotransformed into 200-µl protoplasts and incubated in WI buffer for 12 h. The protoplasts were collected and lysed in 500-µl lysis buffer (0-mM Tris–HCl, 150-mM NaCl, 5-mM EDTA [pH 8.0], 1% NP-40, 0.1-mM PMSF). The extracts were incubated with GFP-Trap agarose beads at 4°C for 3 h and washed three times with washing lysis buffer. Samples were boiled in an SDS protein-loading buffer. Immunoblots were detected by corresponding primary antibodies (anti-GFP, ABclonal no. AE012; anti-Flag, Sigma no. F3165). The primers used for vector construction are shown in **Table S10**.

Dual-Luciferase Reporter assays

The *OsGLK1*, *LHCB4,* and *PORA* promoter sequences were amplified from ZH11 genomic DNA and cloned into the pGreenII 0800-LUC vector (Hellens et al., 2005) as a reporter (pGLK1::LUC, pLHCB4::LUC, pPORA::LUC); the OsGLK1-GFP and OsNF-YB7-Flag constructs as effectors. The reporters and effectors were transfected into rice protoplasts in different combinations and incubated overnight. Firefly LUC and REN activities were measured using the Dual-Luciferase Reporter Assay Kit (Vazyme) following the manufacturer's instructions, and LUC:REN ratios were calculated and presented. The primers used for generating these constructs are listed in **Table S10**.

Chlorophyll measurement and confocal imaging

One hundred micrograms of embryo of the indicated genotypes were extracted in 3 ml of 100% dimethyl sulphoxide (DMSO) and incubated at 65°C for 1 h. Then, the absorbance values at 648.2 and 664.9 nm wavelengths were measured by spectrophotometry, and then total chlorophyll content was calculated (Barnes et al., 1992).

Chlorophyll autofluorescence signal was detected using confocal microscopy (Carl Zeiss, LSM 710), excitation 633 nm; emission 625–730 nm.

Acknowledgments

We thank Prof. Hengxiu Yu and Dr. Chao Zhang for kindly providing the positive and negative control vectors for dual-luciferase reporter assays.

Funding

This research was supported by grants from the National Natural Science Foundation of China (32170344 and 31701392), the Science Fund for Distinguished Young Scholars of Jiangsu Province (BK20180047), the Six Talent Peaks Project in Jiangsu Province (NY-142) and the Priority Academic Development of Jiangsu Higher Education Institutions.

Author contributions

C.C. conceived the project. C.C., B.N., Z.Y., and Q-Q.L. designed the research. B.N., Z.Y., T.B., Z.E., Q.Y, X.X, J.Z., Z.Z. X.L, and Q.L. performed the experiments and analyzed the data. C.C., Z.Y and B.N. wrote the manuscript.

Figure Legends

Figure Legends

Figure 1. Embryogenesis of the WT and *osnf-yb7*

(A–H). The confocal laser scanning microscopy (CLSM) observations of early embryo development of the WT **(A, C, E, G)** and *osnf-yb7* **(B, D, F, H)** at 2- **(A, B)**, 3- **(C, D)**, 4- **(E, F)** and 5 d after fertilization (DAF) **(G, H)**. Scale bars = 100 μm. Sc, scutellum; cp, coleoptile.

(I–P). Scanning electron microscope (SEM) images of the WT **(I—L)** and *osnf-yb7* **(M—P)** embryos at 5- **(I, M, K, O)** and 10 DAF **(J, N, L, P)**. **(K, L, O, P)** are the magnified images of the coleoptile or the life-like structures showed in **(I, J, M, N)**. Scale bars = 100 μm in **(I, J, M, N)**; = 20 μm in **(K, L, O, P)**. Sc, scutellum; cp, coleoptile; su, suspensor; ls, lateral scale; vs, ventral scale; ep, epiblast; ll, leaf-like structure.

(**Q—T).** Vertical **(Q, S)** and horizontal **(R, T)** cross-sections of the early developed embryos of the WT **(Q, R)** and *osnf-yb7* **(S, T)**. From left to right in **(Q, S)**, embryos at 4, 5, 6, 7, and 10 DAF, respectively. From left to right in **(R, T)**, embryos at 4, 5, 6, and 10 DAF, respectively. For the 4-, 5-, 6-, 7-, and 10-DAF-old embryos, scale bars = 50 μm; for the 10-DAF-old embryo, scale bars = 100 μm. Sc, scutellum; cp, coleoptile; cr, coleorhiza; ls, lateral scale; ep, epiblast; ll, leaf-like structure.

Figure 2. Morphologically characterized leaf-like structure of *osnf-yb7* after germination

(A–H). Morphology of the WT coleoptile **(A, B)** and the *osnf-yb7* leaf-like structure **(C, D)** at 120 h after germination. The boxed region in **(A)** and **(C)** is magnified in **(B)** and **(D)**. Scale bars = 1 mm. The dashed lines in **(A, C)** showed the sites of the sections in **(K, L)**.

(E–J). Scanning electron microscopy images of the WT coleoptile **(E, F)**, the WT first leaf **(G, H)**, and the *osnf-yb7* leaf-like structure **(I, J). (E, G, I)** show the tip parts of the tissues; **(F, H, J)** show the epidermal cells of the tissues. Scale bars = 20 μm. White arrows in **(G, I)** indicate hairs derived from the WT first leaf **(G)** and the leaf-like structure of *osnf-yb7* **(I)**; white arrowheads in **(H, J)** indicate trichomes.

(K, L). Horizontal cross-sections of the basal parts, which are indicated by the dashed lines in **(A, C)**, of the WT **(K)** and *osnf-yb7* **(L)** seedlings. Scale bars = 50 μm. Cp, coleoptile; ll, leaf-like structure; L1, the first leaf, L2, the second leaf. Black arrows indicate the vascular bundles.

Figure 3. Transcriptome analysis of the embryos of WT and *osnf-yb7* at 5- and 10 DAF

(A). Venn diagrams of the differentially expressed genes (DEGs) identified from the WT and *osnf-yb7* embryos at 5- and 10 DAF (upper panel), and the developmentally related DEGs (drDEGs) identified from the 5- and 10-DAF-old embryos of the WT and *osnf-yb7* (lower panel).

(B). Heat maps indicate distinct tissue-preferential expression patterns of the top-100 downregulated (left) and upregulated DEGs (right) identified from the 10-DAF-old *osnf-yb7* embryos. The expression data of genes in caryopsis, embryo, endosperm, anther, panicle, seedling, coleoptile, shoot, and root were retrieved from Genevestigator.

(C, D). Many rice embryonic tissue-specific are differentially expressed in the *osnf-yb7* embryos at 5- **(C)** and 10 DAF **(D)**. The scutellum (Sc)-, epiblast (mixture with coleorhiza) (Sc/Cr)-, shoot (Sh)- and root (Rt)-preferential genes were identified by Itoh *et al*. (2016).

(E, F). Enrichment analysis of the differentially expressed transcription factor genes identified from 5- **(E)** and 10-DAF-old **(F)** embryos of *osnf-yb7*. Bubble size indicates the number of differentially expressed transcription factors of the indicated family.

(G). The heat map shows different GO terms were enriched in the up- and downregulated drDEGs identified from the WT and *osnf-yb7* embryos.

(H, I). TTC staining of the 10-DAF-old WT **(H)** and *osnf-yb7* **(I)** seeds. Scale bars = 1 mm.

(J, K). Embryo morphology of the WT **(J)** and *osnf-yb7* **(K)** at □15 DAF. Scale bars = 1 mm.

Figure 4. Loss-of-function of *OsNF-YB7* weakens dormancy

(A). Schematic illustration of the genes involving rice dormancy regulation.

(B). The heat map shows the expression of rice dormancy-related genes in the 5- and 10-DAF-old embryos of WT and *osnf-yb7*.

(C–F). Contents of ABA **(C)**, GA_1 **(D)**, GA_4 **(E),** and the ABA:GA ratio **(F)** in the 10-DAF-old embryos of the WT and *osnf-yb7*. Values are means ± SD of three biological repeats. **, $p < 0.01$ by Student's *t*-test.

(G, H). TTC staining of the mature embryos of the WT **(G)** and *osnf-yb7* **(H)**. Scale bars = 1 mm.

(I, J) Morphology of germinating seeds of the WT (upper) and *osnf-yb7* (lower) at 48 h **(I)** and 120 h **(J)** after imbibition. Scale bars = 5 mm.

Figure 5. OsNF-YB7 negative regulates the expression of chlorophyll biogenesis-associated genes

(A, B). Embryo morphologies of the WT and *osnf-yb7* detached embryos at 8 DAF **(A)** and free-hand dissected embryos at maturation **(B)**. Scale bars = 0.2 mm.

(C, D). Chlorophyll levels in the WT and *osnf-yb7* embryos at ~15 DAF **(C)** and maturation **(D)**.

(E). Heat map of the expression of TFs associates with chlorophyll biogenesis or chloroplast development of the WT and *osnf-yb7*. The color dots indicate $\log_2$(RPKM mean) of the genes in three biological replicates.

(F–H). Expression of *OsGLK1* **(F)**, *OsPIL14* **(G)** and *OsGNC* **(H)** in WT and *osnf-yb7* at 5 DAF. The data are means ± SD of three biological replicates.

(I). The Venn diagram shows overlaps of the upregulated genes in the *osnf-yb7* embryos and in the *OsGLK1* overexpression transgenic plants (OsGLK1-OE). The upregulated genes in OsGLK1-OE were generated by Nakamura *et al.* (2009).

(J, K). Dual-luciferase reporter assays in rice protoplasts showing that OsNF-YB7 represses the activity of GLKpro::LUC. The constructs of reporter and effectors were shown in **(J)**. The data are means ± SD of three biological replicates. **, $p < 0.01$, as determined by Student's *t*-test.

Figure 6. OsNF-YB7 interacts with OsGLK1 to repress the expression of *OsPORA* and *LHCB4*

(A). Y2H assays to test the interactions of OsNF-YB7 with OsGLK1. The indicated combinations of constructs were cotransformed into yeast cells and grown on the nonselective medium SD/-L-T and selective medium SD/-L-T-H and SD/-L-T-H-A.

(B). A split complementary luciferase (LUC) confirmed the interaction between OsNF-YB7 and OsGLK1. Coexpression of the fusion OsGLK1 and the N-terminal half of LUC (GLK1-nLUC) and the fusion of the C-terminal half of LUC and OsNF-YB7 (cLUC-YB7) in the epidermal cells of *N. benthamiana* leaves induced LUC activities, whereas the epidermal cells coexpressed OsGLK1-nLUC and cLUC, nLUC and cLUC-OsNF-YB7, or nLUC and cLUC did not show LUC activities.

(C). BiFC assays showed interactions between OsNF-YB7 and OsGLK1 in nuclei. OsGLK1 was fused with the N-terminal of yellow fluorescent protein (GLK1-nYFP); OsNF-YB7 was fused with the C-terminal of YFP (YB7-cYFP). The recombinant proteins were transiently coexpressed in leaf epidermal cells of *N. benthamiana.* Fluorescence signals indicate that OsGLK1 interacted with OsNF-YB7 in the nuclei.

(D). Co-IP assays showing that OsNF-YB7 interacts with OsGLK1 *in vivo*. 35S::OsNF-YB7:GFP (YB7-GFP) and 35S::OsGLK1:3xFlag (GLK-flag) were coexpressed in rice protoplasts and were immunoprecipitated with an anti-GFP antibody, and the immunoblots were probed with anti-GFP and anti-Flag antibodies. 35S::GFP (GFP) was a negative control.

(E, F). Expression of *LHCB4* **(E)** and *OsPORA* **(F)** was activated in the embryos of *osnf-yb7* at 10 DAF.

(G). Schematic diagrams of various constructs used in dual-luciferase reporter assays. LUC, firefly luciferase; REN, Renilla luciferase.

(H, I). Dual-luciferase reporter assays in rice protoplasts showing that OsNF-YB7 represses the activation of the *LHCB4pro::LUC* **(H)** and *PORApro::LUC* **(I)** reporters by OsGLK1. The LUC:REN ratio represents the LHCB4pro:LUC and PORApro:LUC activity relative to the internal control. Data are means ± SD of three biological replicates. **, $p < 0.01$, as determined by Student's *t*-test.

(J–M). Morphologies of the embryos produced by WT **(J)**, *osnf-yb7* **(K)**, *osnf-yb7;osglk2* double mutant **(L),** and *osnf-yb7;osglk1;osglk2* triple mutant **(M)**. Scale bars = 0.2 mm.

Figure 7. The maize OsNF-YB7 homologs play a similar role in embryo development

(A). The neighbor-joint tree and expressed preference of the LEC1-type genes in Arabidopsis, rice, and maize.

(B). Growth retardation showed in the maize *lec1* (double mutant of Zm00001d051697 and Zm00001d017898) mutant (right) when compared with the WT (left).

(C, D). Free-hand vertical sections of the mature WT **(C)** and maize *lec1* **(D)** embryos. Scale bars = 1 mm. Sc, scutellum; cp, coleoptile; el, epiblast-like structure; cr, coleorhiza; pl, plumule; ra, radicle; ll, leaf-like structure.

(E, F). The germinated embryos of WT **(E)** and maize *lec1* **(F)** after 3 d water imbibition. Scale bars = 1 mm. Cp, coleoptile; el, epiblast-like structure; ra, radicle; ll, leaf-like structure.

(G, H). Free-hand vertical sections of the germinated WT **(G)** and maize *lec1* **(H)** embryos after 48 h water imbibition. Scale bars = 1 mm. Sc, scutellum; cp, coleoptile; el, epiblast-like structure; pl, plumule; ll, leaf-like structure.

(I, J). The side view **(I)** and vertical view **(J)** of the detached germinated embryos of the WT and maize *lec1*. Scale bars = 1 mm. Sc, scutellum; cp, coleoptile; ra, radicle; ll, leaf-like structure.

(K, L). Free-hand vertical sections of the detached WT **(K)** and maize *lec1* **(L)** germinated embryos at 7 d after germination. Scale bars = 1 mm. Sc, scutellum; cp, coleoptile; el, epiblast-like structure; pl, plumule; ll, leaf-like structure.

Figure 8. Schematic illustration of the functional conservation between Arabidopsis *LEC1* and rice *OsNF-YB7* for embryo development

Both Arabidopsis *lec1* and rice *osnf-yb7* mutants show defects of embryogenesis, maturation, and dormancy. Notably, like that observed in the *lec1* cotyledons, the embryonic envelope of *osnf-yb7* developed into a leaf-like structure with somewhat true-leaf identities. Additionally, the rice *osnf-yb7* develops chloroembryos, due to a chlorophyll-biogenesis activation in the embryo. However, the *lec1* seed showed paler green coloration than the WT.

Supplemental Figure 1. Seed and embryo morphologies of the WT and two independent mutant lines of *osnf-yb7*

Supplemental Figure 2. Histological analysis of the embryos of the WT and *osnf-yb7*.

Supplemental Figure 3. Relative expression of rice dormancy-related genes and ABA responsive genes in the 10-DAF-old WT and *osnf-yb7* embryos

Supplemental Figure 4. Relative expression of GA metabolic and responsive genes in the osnf-yb7 embryos.

Supplemental Figure 5. Expression of late embryogenesis abundant (LEA) genes in the embryos of WT and *osnf-yb7*

Supplemental Figure 6. Chlorophyll biosynthesis was activated in the embryos of *osnf-yb7*

Supplemental Figure 7. Photosynthesis related MapMAN pathways were enriched for the differential expressed genes (DEGs) identified from the *osnf-yb7* embryos

Supplemental Figure 8. Generation of *osnf-yb7*, *osglk1* and *osglk2* high-order mutants

Supplemental Figure 9. Generation of maize *lec1* mutants

Supplemental Figure 10. Light is required for chlorophyll biosynthesis in the chloroembryos produced by *osnf-yb7*

Supplemental Figure 11. The endosperm development was not largely affected in *osnf-yb7*

Supplemental Figure 12. Schematic illustration the homologies of the rice embryonic structures

Supplemental Figure 13. Principle component analysis of the transcriptome profiles of the scutellum, epiblast/coleorhiza mixture, shoot, and root of the embryo in rice

Supplemental Figure 14. Schematic illustration the OsNF-YB7 regulated chlorophyll biosynthesis in the embryo of rice

Supplemental Table 1. Differentially expressed genes in the 5-DAF-old embryos of *osnf-yb7*.

Supplemental Table 1. Differentially expressed genes in the 10-DAF-old embryos of *osnf-yb7*.

Supplemetal Table 3. Differential expression of the embyonic tissue specific genes in *osnf-yb7*

Supplemental Table 4. Differentially expressed transcription factors in the *osnf-yb7* embryos.

Supplemental Table 5. Development related differentially expressed genes identified between the 5- and 10-DAF-old WT embryos.

Supplemental Table 6. Development related differentially expressed genes identified between the 5- and 10-DAF-old *osnf-yb7* embryos.

Supplemental Table 7. Expression of the ABA-metabolic and responsive genes in the WT and *osnf-yb7* embryos.

Supplemental Table 8. Expression of the ABA-metabolic and responsive genes in the WT and *osnf-yb7* embryos.

Supplemental Table 9. Differentially expressed genes in the 10-DAF-old emdosperm of *osnf-yb7*.

Supplemental Table 10. Primers used for the present study

References

Armenta-Medina, A., Gillmor, C.S., Gao, P., Mora-Macias, J., Kochian, L. V., Xiang, D., and Datla, R. (2021). Developmental and genomic architecture of plant embryogenesis: from model plant to crops. Plant Commun. **2**: 100136.

Bai, B., Lu, N., Li, Y., Guo, S., Yin, H., He, Y., Sun, W., Li, W., and Xie, X. (2019). OsBBX14 promotes photomorphogenesis in rice by activating OsHY5L1 expression under blue light conditions. Plant Sci. **284**: 192–202.

Barnes, J.D., Balaguer, L., Manrique, E., Elvira, S., and Davison, A.W. (1992). A reappraisal of the use of DMSO for the extraction and determination of chlorophylls a and b in lichens and higher plants. Environ. Exp. Bot. **32**: 85–100.

Boulard, C., Fatihi, A., Lepiniec, L., and Dubreucq, B. (2017). Regulation and evolution of the interaction of the seed B3 transcription factors with NF-Y subunits. Biochim. Biophys. Acta - Gene Regul. Mech. **1860**: 1069–1078.

Brown, W. (1965). The Grass Embryo-A Rebutal. Phytomorphology: 275–284.

Brown, W. (1960). The morphology of the grass embryo. Phytomorphology: 215–223.

Cagliari, A., Turchetto-Zolet, A.C., Korbes, A.P., Maraschin, F. dos S., Margis, R., and Margis-Pinheiro, M. (2014). New insights on the evolution of Leafy cotyledon1 (LEC1) type genes in vascular plants. Genomics **103**: 380–387.

797 Chandler, J.W. (2008). Cotyledon organogenesis. J. Exp. Bot. 59: 2917–2931.

798 Chen, C., Chen, H., Zhang, Y., Thomas, H.R., Frank, M.H., He, Y., and Xia, R. (2020).
799 TBtools: An Integrative Toolkit Developed for Interactive Analyses of Big Biological Data. Mol.
800 Plant 13: 1194–1202.

801 Chen, W., Wang, W., Lyu, Y., Wu, Y., Huang, P., Hu, S., Wei, X., Jiao, G., Sheng, Z.,
802 Tang, S., Shao, G., and Luo, J. (2021). OsVP1 activates Sdr4 expression to control rice
803 seed dormancy via the ABA signaling pathway. Crop J. 9: 68–78.

804 Cheng, X., Pan, M., E, Z., Zhou, Y., Niu, B., and Chen, C. (2020). The Maternally
805 Expressed Polycomb Group Gene OsEMF2a Is Essential for Endosperm Cellularization and
806 Imprinting in Rice. Plant Commun. 2: 100092.

807 Du, Z., Zhou, X., Ling, Y., Zhang, Z., and Su, Z. (2010). agriGO: a GO analysis toolkit for the
808 agricultural community. Nucleic Acids Res. 38: W64–W70.

809 E, Z., Li, T., Zhang, H., Liu, Z., Deng, H., Sharma, S., Wei, X., Wang, L., Niu, B., and
810 Chen, C. (2018). A group of nuclear factor Y transcription factors are sub-functionalized
811 during endosperm development in monocots. J. Exp. Bot. 69: 2495–2510.

812 Gaj, M.D., Zhang, S., Harada, J.J., and Lemaux, P.G. (2005). Leafy cotyledon genes are
813 essential for induction of somatic embryogenesis of Arabidopsis. Planta 222: 977–988.

814 Guo, X., Hou, X., Fang, J., Wei, P., Xu, B., Chen, M., Feng, Y., and Chu, C. (2013). The
815 rice GERMINATION DEFECTIVE 1 , encoding a B3 domain transcriptional repressor, regulates
816 seed germination and seedling development by integrating GA and carbohydrate
817 metabolism. Plant J. 75: 403–416.

818 Harada, J.J. (2001). Role of arabidopsis LEAFY COTYLEDON genes in seed development. J. Plant
819 Physiol. 158: 405–409.

820 He, Y. and Niu, D. (2019). LEAFY COTYLEDONs: Old genes with new roles beyond seed
821 development. F1000Research 8: 1–7.

822 Hellens, R.P., Allan, A.C., Friel, E.N., Bolitho, K., Grafton, K., Templeton, M.D.,
823 Karunairetnam, S., Gleave, A.P., and Laing, W.A. (2005). Transient expression
824 vectors for functional genomics, quantification of promoter activity and RNA silencing in
825 plants. Plant Methods 1: 1–14.

826 Hibara, K. ichiro, Obara, M., Hayashida, E., Abe, M., Ishimaru, T., Satoh, H., Itoh, J.
827 ichi, and Nagato, Y. (2009). The ADAXIALIZED LEAF1 gene functions in leaf and
828 embryonic pattern formation in rice. Dev. Biol. 334: 345–354.

829 Hong, S.-K., Aoki, T., Kitano, H., Satoh, H., and Nagato, Y. (1995). Phenotypic diversity
830 of 188 rice embryo mutants. Dev. Genet. 16: 298–310.

831 Hu, Y., Zhou, L., Huang, M., He, X., Yang, Y., Liu, X., Li, Y., and Hou, X. (2018).
832 Gibberellins play an essential role in late embryogenesis of Arabidopsis. Nat. Plants 4: 289–
833 298.

834 Huang, M., Hu, Y., Liu, X., Li, Y., and Hou, X. (2015a). Arabidopsis LEAFY COTYLEDON1

controls cell fate determination during post-embryonic development. Front. Plant Sci. **6**: 955.

Huang, M., Hu, Y., Liu, X., Li, Y., and Hou, X. (2015b). Arabidopsis LEAFY COTYLEDON1 mediates postembryonic development via interacting with PHYTOCHROME-INTERACTING FACTOR4. Plant Cell **27**: 3099–3111.

Huang, X., Peng, X., and Sun, M.X. (2017). OsGCD1 is essential for rice fertility and required for embryo dorsal-ventral pattern formation and endosperm development. New Phytol. **215**: 1039–1058.

Ishimoto, K. et al. (2019). Specification of basal region identity after asymmetric zygotic division requires mitogen-activated protein kinase 6 in rice. Development **146**: dev176305.

Ito, Y., Thirumurugan, T., Serizawa, A., Hiratsu, K., Ohme-Takagi, M., and Kurata, N. (2011). Aberrant vegetative and reproductive development by overexpression and lethality by silencing of OsHAP3E in rice. Plant Sci. **181**: 105–110.

Itoh, J.-I., Sato, Y., Sato, Y., Hibara, K.-I., Shimizu-Sato, S., Kobayashi, H., Takehisa, H., Sanguinet, K.A., Namiki, N., and Nagamura, Y. (2016). Genome-wide analysis of spatio-temporal gene expression patterns during early embryogenesis in rice. Development **143**: 1217–1227.

Itoh, J., Nonomura, K., Ikeda, K., Yamaki, S., Inukai, Y., Yamagishi, H., Kitano, H., and Nagato, Y. (2005). Rice Plant Development: from Zygote to Spikelet. Plant Cell Physiol. **46**: 23–47.

Jarvis, P. and López-Juez, E. (2013). Biogenesis and homeostasis of chloroplasts and other plastids. Nat. Rev. Mol. Cell Biol. **14**: 787–802.

Jo, L., Pelletier, J.M., and Harada, J.J. (2019). Central role of the LEAFY COTYLEDON1 transcription factor in seed development. J. Integr. Plant Biol. **61**: 564–580.

Jo, L., Pelletier, J.M., Hsu, S., Baden, R., Goldberg, R.B., and Harada, J.J. (2020). Combinatorial interactions of the LEC1 transcription factor specify diverse developmental programs during soybean seed development. Proc. Natl. Acad. Sci. **117**: 1223–1232.

Lee, H., Fischer, R.L., Goldberg, R.B., and Harada, J.J. (2003). Arabidopsis LEAFY COTYLEDON1 represents a functionally specialized subunit of the CCAAT binding transcription factor. Proc. Natl. Acad. Sci. U. S. A. **100**: 2152–6.

Lepiniec, L., Devic, M., Roscoe, T.J., Bouyer, D., Zhou, D.X., Boulard, C., Baud, S., and Dubreucq, B. (2018). Molecular and epigenetic regulations and functions of the LAFL transcriptional regulators that control seed development. Plant Reprod. **31**: 291–307.

Li, Z., Mo, W., Jia, L., Xu, Y.C., Tang, W., Yang, W., Guo, Y.L., and Lin, R. (2019). Rice FLUORESCENT1 Is Involved in the Regulation of Chlorophyll. Plant Cell Physiol. **60**: 2307–2318.

Lotan, T., Ohto, M., Yee, K.M., West, M.A.L., Lo, R., Kwong, R.W., Yamagishi, K., Fischer, R.L., Goldberg, R.B., and Harada, J.J. (1998). Arabidopsis LEAFY

873 COTYLEDON1 is sufficient to induce embryo development in vegetative cells. Cell **93**: 1195–
874 1205.

875 **Meinke, D.W.** (1992). A Homoeotic Mutant of Arabidopsis thaliana with Leafy Cotyledons.
876 Science **258**: 1647–50.

877 **Meinke, D.W., Franzmann, L.H., Nickle, T.C., and Yeung, E.C.** (1994). Leafy cotyledon
878 mutants of Arabidopsis. Plant Cell **6**: 1049–1064.

879 **Miyoshi, K., Ito, Y., Serizawa, A., and Kurata, N.** (2003). OsHAP3 genes regulate
880 chloroplast biogenesis in rice. Plant J. **36**: 532–540.

881 **Morita, A., Umemura, T.A., Kuroyanagi, M., Futsuhara, Y., Perata, P., and**
882 **Yamaguchi, J.** (1998). Functional dissection of a sugar-repressed α-amylase gene (RAmy1A)
883 promoter in rice embryos. FEBS Lett. **423**: 81–85.

884 **Mu, J. et al.** (2008). LEAFY COTYLEDON1 Is a Key Regulator of Fatty Acid Biosynthesis in
885 Arabidopsis. Plant Physiol. **148**: 1042–1054.

886 **Nagato, Y., Kitano, H., Kamijima, O., Kikuchi, S., and Satoh, H.** (1989). Developmental
887 mutants showing abnormal organ differentiation in rice embryos. Theor. Appl. Genet. **78**:
888 11–15.

889 **Nagatoshi, Y., Mitsuda, N., Hayashi, M., Inoue, S.I., Okuma, E., Kubo, A., Murata, Y.,**
890 **Seo, M., Saji, H., Kinoshita, T., and Ohme-Takagi, M.** (2016). GOLDEN 2-LIKE
891 transcription factors for chloroplast development affect ozone tolerance through the
892 regulation of stomatal movement. Proc. Natl. Acad. Sci. U. S. A. **113**: 4218–4223.

893 **Nakamura, H., Muramatsu, M., Hakata, M., Ueno, O., Nagamura, Y., Hirochika, H.,**
894 **Takano, M., and Ichikawa, H.** (2009). Ectopic overexpression of the transcription factor
895 osglk1 induces chloroplast development in non-green rice cells. Plant Cell Physiol. **50**: 1933–
896 1949.

897 **Niu, B., Deng, H., Li, T., Sharma, S., Yun, Q., Li, Q., E, Z., and Chen, C.** (2020).
898 OsbZIP76 interacts with OsNF-YBs and regulates endosperm cellularization in rice (Oryza
899 sativa). J. Integr. Plant Biol. **62**: 1983–1996.

900 **Niu, B., Zhang, Z., Zhang, J., Zhou, Y., and Chen, C.** (2021). The rice LEC1-like
901 transcription factor OsNF-YB9 interacts with SPK, an endosperm-specific sucrose synthase
902 protein kinase, and functions in seed development. Plant J.: 1233–1246.

903 **Nosaka, M., Nagasaki, H., Mukouhata, M., Hibara, K. -i., Sato, Y., Ashikari, M.,**
904 **Nagato, Y., Hayashi, K., Itoh, J. -i., Satoh-Nagasawa, N., Kitano, H., and**
905 **Matsuoka, M.** (2007). The small interfering RNA production pathway is required for shoot
906 meristem initiation in rice. Proc. Natl. Acad. Sci. **104**: 14867–14871.

907 **Parcy, F., Valon, C., Kohara, A., Miséra, S., and Giraudat, J.** (1997). The ABSCISIC
908 ACID-INSENSITIVE3, FUSCA3, and LEAFY COTYLEDON1 loci act in concert to control multiple
909 aspects of arabidopsis seed development. Plant Cell **9**: 1265–1277.

910 **Pelletier, J.M., Kwong, R.W., Park, S., Le, B.H., Baden, R., Cagliari, A., Hashimoto,**

M., Munoz, M.D., Fischer, R.L., Goldberg, R.B., and Harada, J.J. (2017). LEC1 sequentially regulates the transcription of genes involved in diverse developmental processes during seed development. Proc. Natl. Acad. Sci. 114: E6710–E6719.

Puthur, J.T., Shackira, A.M., Saradhi, P.P., and Bartels, D. (2013). Chloroembryos: A unique photosynthesis system. J. Plant Physiol. 170: 1131–1138.

Qi, D., Wen, Q., Meng, Z., Yuan, S., Guo, H., Zhao, H., and Cui, S. (2020). OsLFR is essential for early endosperm and embryo development by interacting with SWI/SNF complex members in Oryza sativa. Plant J. 104: 901–916.

Sakuraba, Y., Kim, E.Y., Han, S.H., Piao, W., An, G., Todaka, D., Yamaguchi-Shinozaki, K., and Paek, N.C. (2017). Rice Phytochrome-Interacting Factor-Like1 (OsPIL1) is involved in the promotion of chlorophyll biosynthesis through feed-forward regulatory loops. J. Exp. Bot. 68: 4103–4114.

Sato, Y., Hibara, K.-I., Nagamura, Y., Takehisa, H., Shimizu-Sato, S., Sanguinet, K.A., Itoh, J.-I., Namiki, N., and Kobayashi, H. (2016). Genome-wide analysis of spatiotemporal gene expression patterns during early embryogenesis in rice. Development 143: 1217–1227.

Satoh, N., Hong, S.K., Nishimura, A., Matsuoka, M., Kitano, H., and Nagato, Y. (1999). Initiation of shoot apical meristem in rice: Characterization of four SHOOTLESS genes. Development 126: 3629–3636.

Satoh, N., Itoh, J.I., and Nagato, Y. (2003). The SHOOTLESS2 and SHOOTLESS1 genes are involved in both initiation and maintenance of the shoot apical meristem through regulating the number of indeterminate cells. Genetics 164: 335–346.

Sazuka, T., Kamiya, N., Nishimura, T., Ohmae, K., Sato, Y., Imamura, K., Nagato, Y., Koshiba, T., Nagamura, Y., Ashikari, M., Kitano, H., and Matsuoka, M. (2009). A rice tryptophan deficient dwarf mutant, tdd1, contains a reduced level of indole acetic acid and develops abnormal flowers and organless embryos. Plant J. 60: 227–241.

Simkin, A.J., Faralli, M., Ramamoorthy, S., and Lawson, T. (2020). Photosynthesis in non-foliar tissues: implications for yield. Plant J. 101: 1001–1015.

Smolikova, G., Dolgikh, E., Vikhnina, M., Frolov, A., and Medvedev, S. (2017). Genetic and hormonal regulation of chlorophyll degradation during maturation of seeds with green embryos. Int. J. Mol. Sci. 18: 5–10.

Smolikova, G.N. and Medvedev, S.S. (2016). Photosynthesis in the seeds of chloroembryophytes. Russ. J. Plant Physiol. 63: 1–12.

Sugimoto, K., Takeuchi, Y., Ebana, K., Miyao, A., Hirochika, H., Hara, N., Ishiyama, K., Kobayashi, M., Ban, Y., Hattori, T., and Yano, M. (2010). Molecular cloning of Sdr4, a regulator involved in seed dormancy and domestication of rice. Proc. Natl. Acad. Sci. U. S. A. 107: 5792–5797.

Tao, Z., Shen, L., Gu, X., Wang, Y., Yu, H., and He, Y. (2017). Embryonic epigenetic reprogramming by a pioneer transcription factor in plants. Nature.

Usadel, B., Poree, F., Nagel, A., Lohse, M., Czedik-Eysenberg, A., and Stitt, M. (2009). A guide to using MapMan to visualize and compare Omics data in plants: A case study in the crop species, Maize. Plant, Cell Environ. **32**: 1211–1229.

Wang, J., Deng, Q., Li, Y., Yu, Y., Liu, X., Han, Y., Luo, X., Wu, X., Ju, L., Sun, J., Liu, A., and Fang, J. (2020). Transcription Factors Rc and OsVP 1 Coordinately Regulate Preharvest Sprouting Tolerance in Red Pericarp Rice. J. Agric. Food Chem. **68**: 14748–14757.

Wang, P., Fouracre, J., Kelly, S., Karki, S., Gowik, U., Aubry, S., Shaw, M.K., Westhoff, P., Slamet-Loedin, I.H., Quick, W.P., Hibberd, J.M., and Langdale, J.A. (2013). Evolution of GOLDEN2-LIKE gene function in C3 and C4 plants. Planta **237**: 481–495.

Waters, M.T., Wang, P., Korkaric, M., Capper, R.G., Saunders, N.J., and Langdale, J.A. (2009). GLK transcription factors coordinate expression of the photosynthetic apparatus in Arabidopsis. Plant Cell **21**: 1109–1128.

West, M.A.L., Yee, K.M., Danao, J., Zimmerman, J.L., Fischer, R.L., Goldberg, R.B., and Harada, J.J. (1994). LEAFY COTYLEDON1 is an essential regulator of late embryogenesis and cotyledon identity in Arabidopsis. Plant Cell **6**: 1731–1745.

Xie, X., Chen, C., Shu, J., Thapa, R.K., Kohalmi, S.E., Marsolais, F., and Zou, J. (2021). LEAFY COTYLEDON1 expression in the endosperm enables embryo maturation in Arabidopsis. Nat. Commun.

Xie, Z., Li, X., Glover, B.J., Bai, S., Rao, G.Y., Luo, J., and Yang, J. (2008). Duplication and functional diversification of HAP3 genes leading to the origin of the seed-developmental regulatory gene, LEAFY COTYLEDON1 (LEC1), in nonseed plant genomes. Mol. Biol. Evol. **25**: 1581–1592.

Xu, X. Bin, Han, H.Z., Liu, X.D., Xu, S.X., Yang, J.F., and Yeung, E. (1999). The tridimensional morphology of rice embryo development with special reference to the scutellum and the coleoptile. Acta Bot. Sin. **41**: 472–478.

Yi, J., Lee, Y.-S., Lee, D.-Y., Cho, M.-H., Jeon, J.-S., and An, G. (2016). OsMPK6 plays a critical role in cell differentiation during early embryogenesis in Oryza sativa. J. Exp. Bot. **67**: 2425–2437.

Zhang, C., Zhang, J., Tang, Y., Liu, K., Liu, Y., Tang, J., Zhang, T., and Yu, H. (2021). DEEP GREEN PANICLE1 suppresses GOLDEN2-LIKE activity to reduce chlorophyll synthesis in rice glumes. Plant Physiol. **185**: 469–477.

Zhang, J.-J. and Xue, H.-W. (2013). OsLEC1/OsHAP3E participates in the determination of meristem identity in both vegetative and reproductive developments of rice. J. Integr. Plant Biol. **55**: 232–49.

Zhang, Y., Su, J., Duan, S., Ao, Y., Dai, J., Liu, J., Wang, P., Li, Y., Liu, B., Feng, D., Wang, J., and Wang, H. (2011). A highly efficient rice green tissue protoplast system for transient gene expression and studying light/chloroplast-related processes. Plant Methods **7**: 1–14.

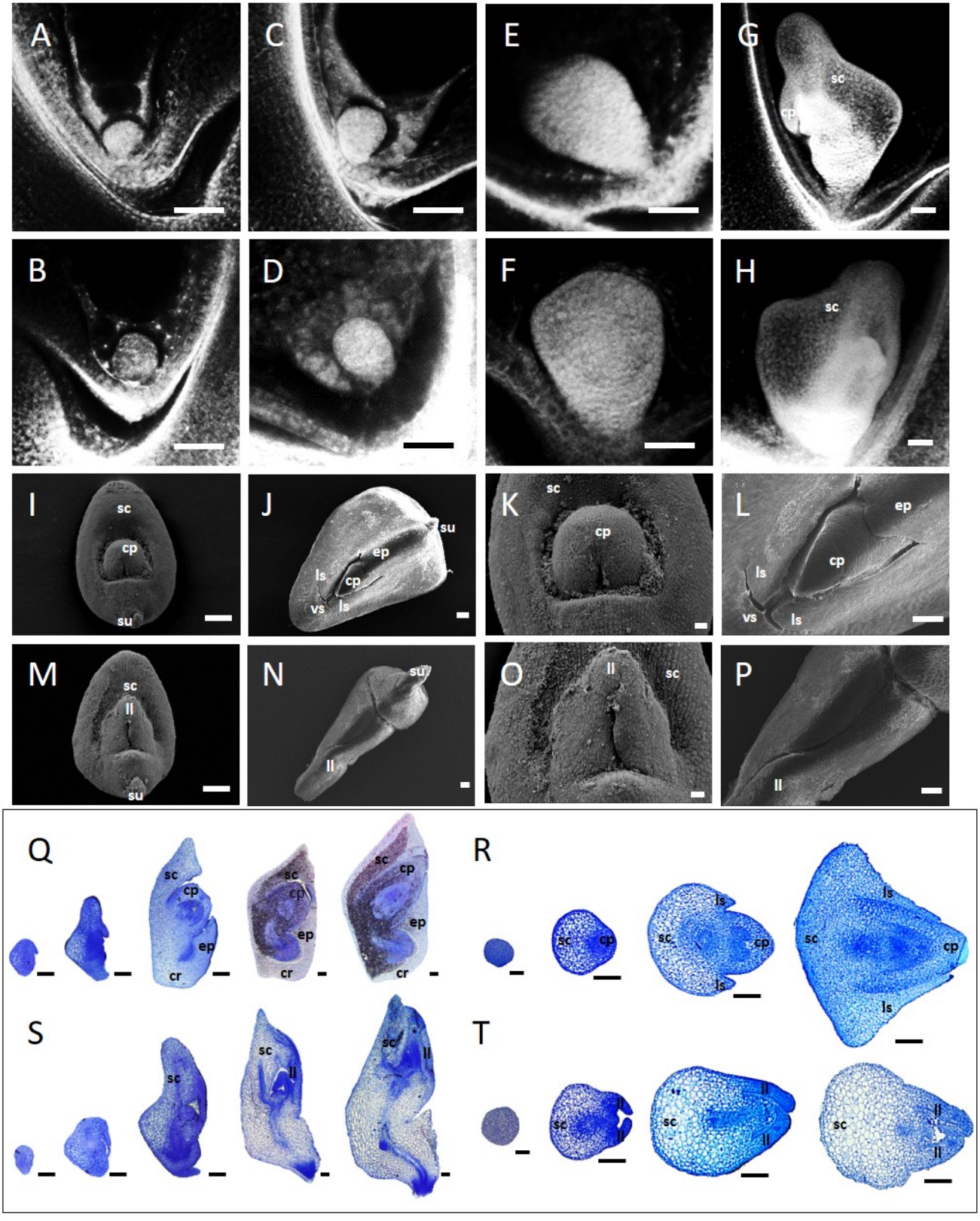

Figure 1. Embryogenesis of the WT and *osnf-yb7*

(A–H). The confocal laser scanning microscopy (CLSM) observations of early embryo development of the WT **(A, C, E, G)** and *osnf-yb7* **(B, D, F, H)** at 2- **(A, B)**, 3- **(C, D)**, 4- **(E, F)** and 5 d after fertilization (DAF) **(G, H).** Scale bars = 100 μm. Sc, scutellum; cp, coleoptile.

(I–P). Scanning electron microscope (SEM) images of the WT **(I—L)** and *osnf-yb7* **(M—P)** embryos at 5- **(I, M, K, O)** and 10 DAF **(J, N, L, P)**. **(K, L, O, P)** are the magnified images of the coleoptile or the life-like structures showed in **(I, J, M, N)**. Scale bars = 100 μm in **(I, J, M, N)**; = 20 μm in **(K, L, O, P)**. Sc, scutellum; cp, coleoptile; su, suspensor; ls, lateral scale; vs, ventral scale; ep, epiblast; ll, leaf-like structure.

(Q—T). Vertical **(Q, S)** and horizontal **(R, T)** cross-sections of the early developed embryos of the WT **(Q, R)** and *osnf-yb7* **(S, T)**. From left to right in **(Q, S)**, embryos at 4, 5, 6, 7, and 10 DAF, respectively. From left to right in **(R, T)**, embryos at 4, 5, 6, and 10 DAF, respectively. For the 4-, 5-, 6-, 7-, and 10-DAF-old embryos, scale bars = 50 μm; for the 10-DAF-old embryo, scale bars = 100 μm. Sc, scutellum; cp, coleoptile; cr, coleorhiza; ls, lateral scale; ep, epiblast; ll, leaf-like structure.

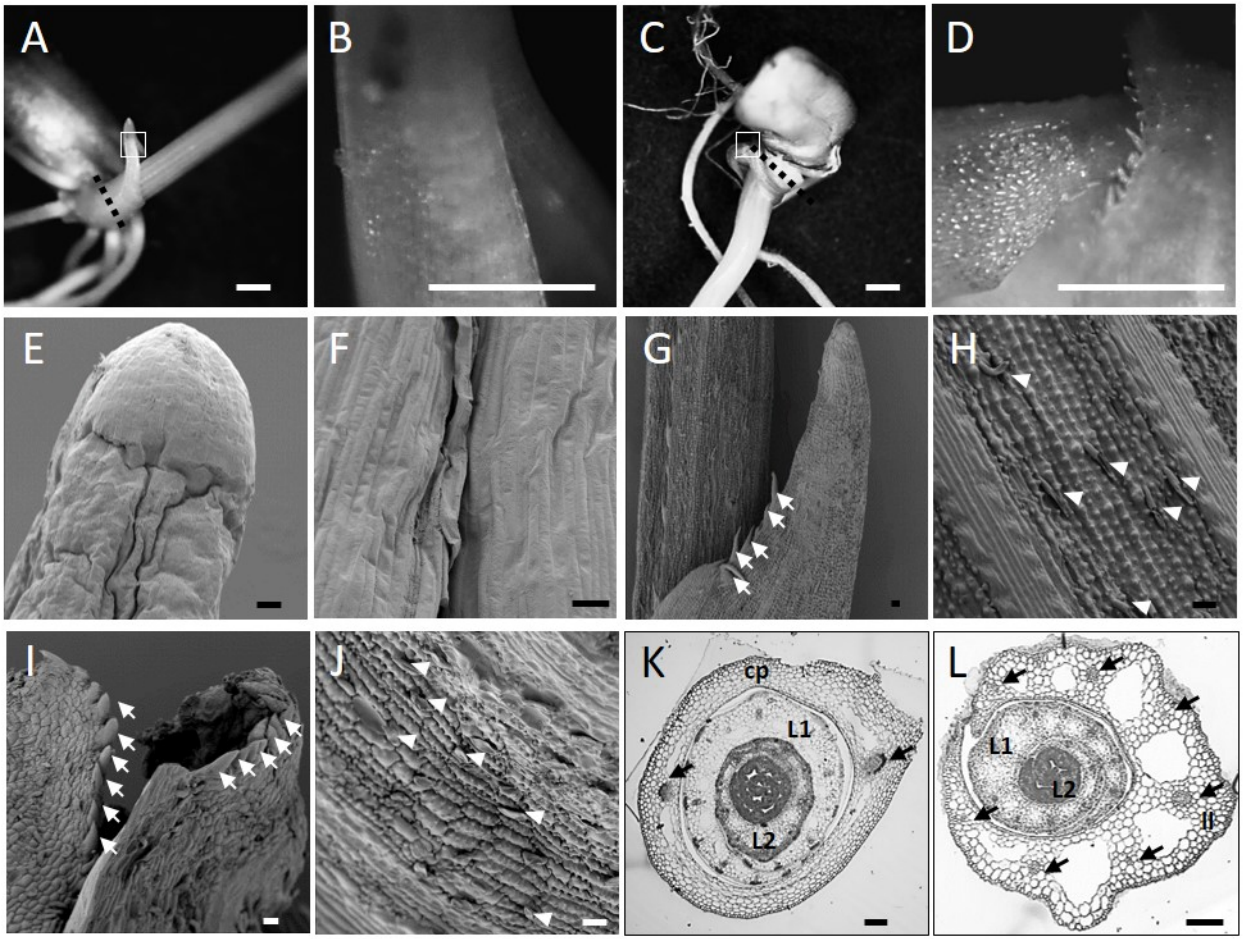

Figure 2. Morphologically characterized leaf-like structure of *osnf-yb7* after germination

(A–H). Morphology of the WT coleoptile **(A, B)** and the *osnf-yb7* leaf-like structure **(C, D)** at 120 h after germination. The boxed region in **(A)** and **(C)** is magnified in **(B)** and **(D)**. Scale bars = 1 mm. The dashed lines in **(A, C)** showed the sites of the sections in **(K, L)**.

(E–J). Scanning electron microscopy images of the WT coleoptile **(E, F)**, the WT first leaf **(G, H)**, and the *osnf-yb7* leaf-like structure **(I, J)**. **(E, G, I)** show the tip parts of the tissues; **(F, H, J)** show the epidermal cells of the tissues. Scale bars = 20 μm. White arrows in **(G, I)** indicate hairs derived from the WT first leaf **(G)** and the leaf-like structure of *osnf-yb7* **(I)**; white arrowheads in **(H, J)** indicate trichomes.

(K, L). Horizontal cross-sections of the basal parts, which are indicated by the dashed lines in **(A, C)**, of the WT **(K)** and *osnf-yb7* **(L)** seedlings. Scale bars = 50 μm. Cp, coleoptile; ll, leaf-like structure; L1, the first leaf, L2, the second leaf. Black arrows indicate the vascular bundles.

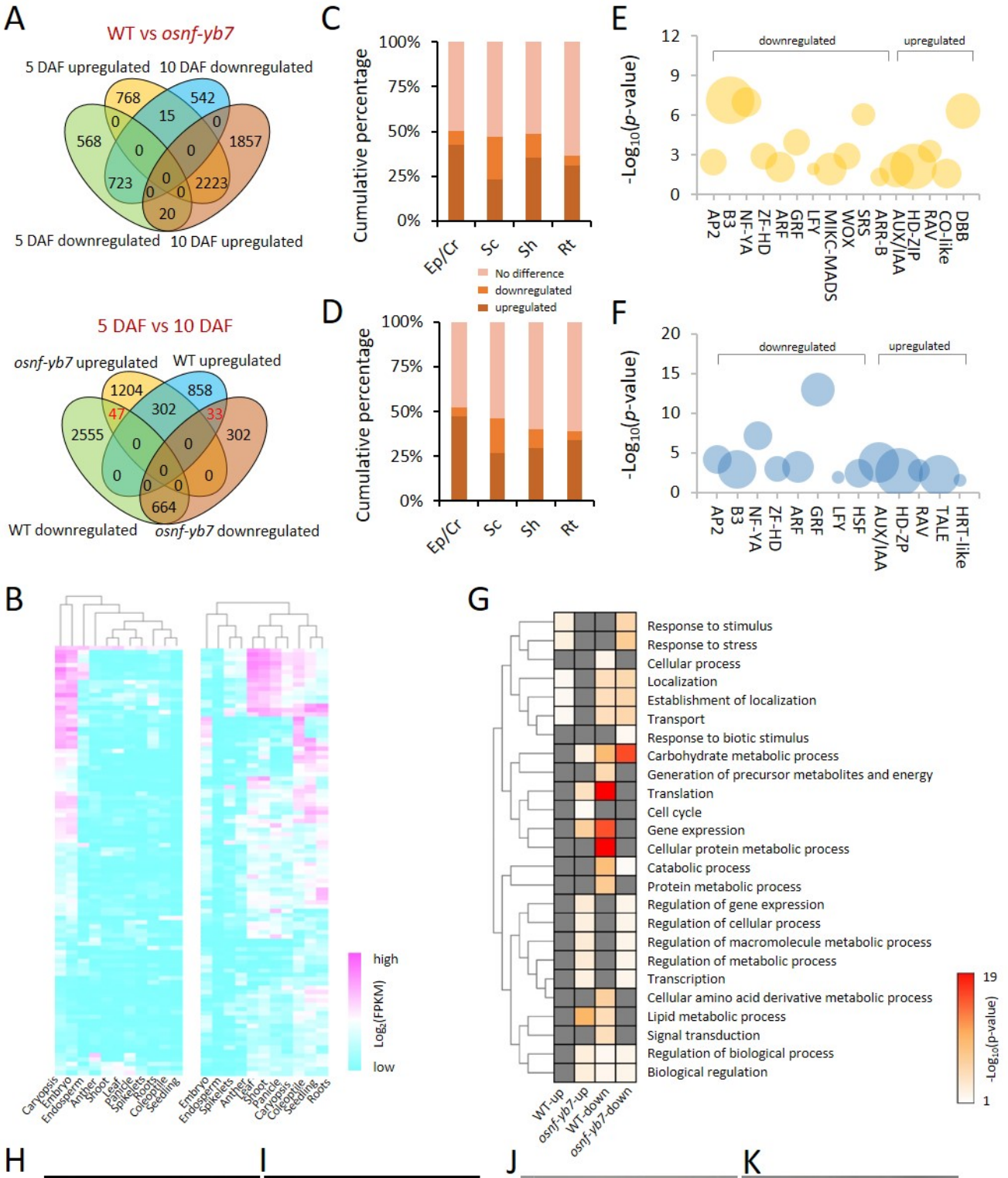

Figure 3. Transcriptome analysis of the embryos of WT and *osnf-yb7* at 5- and 10 DAF

(A). Venn diagrams of the differentially expressed genes (DEGs) identified from the WT and *osnf-yb7* embryos at 5- and 10 DAF (upper panel), and the developmentally related DEGs (drDEGs) identified from the 5- and 10-DAF-old embryos of the WT and *osnf-yb7* (lower panel).

(B). Heat maps indicate distinct tissue-preferential expression patterns of the top-100 downregulated (left) and upregulated DEGs (right) identified from the 10-DAF-old *osnf-yb7* embryos. The expression data of genes in caryopsis, embryo, endosperm, anther, panicle, seedling, coleoptile, shoot, and root were retrieved from Genevestigator.

(C, D). Many rice embryonic tissue-specific are differentially expressed in the *osnf-yb7* embryos at 5- **(C)** and 10 DAF **(D)**. The scutellum (Sc)-, epiblast (mixture with coleorhiza) (Sc/Cr)-, shoot (Sh)- and root (Rt)-preferential genes were identified by Itoh *et al*. (2016).

(E, F). Enrichment analysis of the differentially expressed transcription factor genes identified from 5- **(E)** and 10-DAF-old **(F)** embryos of *osnf-yb7*. Bubble size indicates the number of differentially expressed transcription factors of the indicated family.

(G). The heat map shows different GO terms were enriched in the up- and downregulated drDEGs identified from the WT and *osnf-yb7* embryos.

(H, I). TTC staining of the 10-DAF-old WT **(H)** and *osnf-yb7* **(I)** seeds. Scale bars = 1 mm.

(J, K). Embryo morphology of the WT **(J)** and *osnf-yb7* **(K)** at ~15 DAF. Scale bars = 1 mm.

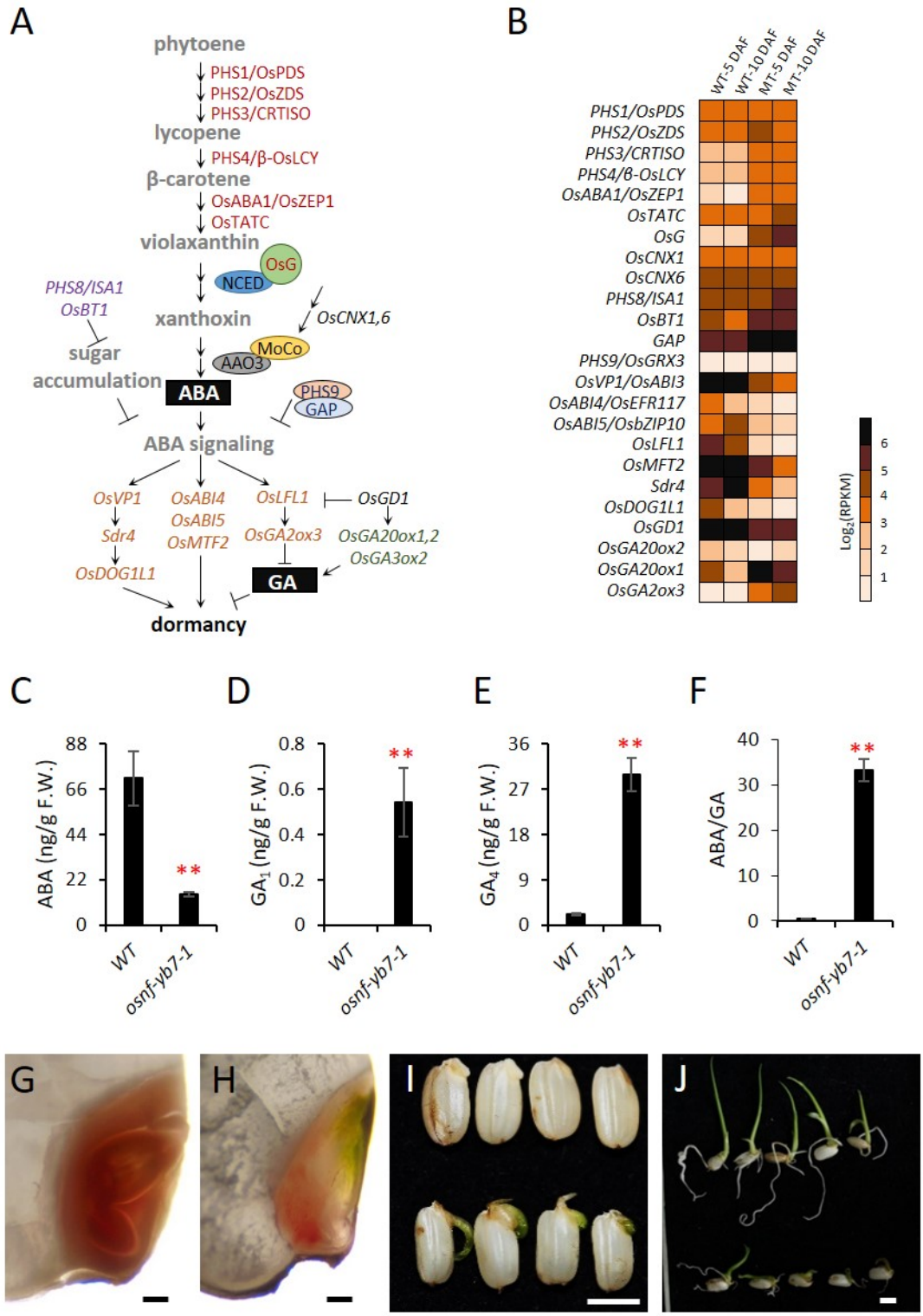

Figure 4. Loss-of-function of *OsNF-YB7* weakens dormancy

(A). Schematic illustration of the genes involving rice dormancy regulation.

(B). The heat map shows the expression of rice dormancy-related genes in the 5- and 10-DAF-old embryos of WT and *osnf-yb7*.

(C–F). Contents of ABA **(C)**, GA_1 **(D)**, GA_4 **(E),** and the ABA:GA ratio **(F)** in the 10-DAF-old embryos of the WT and *osnf-yb7*. Values are means ± SD of three biological repeats. **, $p < 0.01$ by Student's *t*-test.

(G, H). TTC staining of the mature embryos of the WT **(G)** and *osnf-yb7* **(H)**. Scale bars = 1 mm.

(I, J) Morphology of germinating seeds of the WT (upper) and *osnf-yb7* (lower) at 48 h **(I)** and 120 h **(J)** after imbibition. Scale bars = 5 mm.

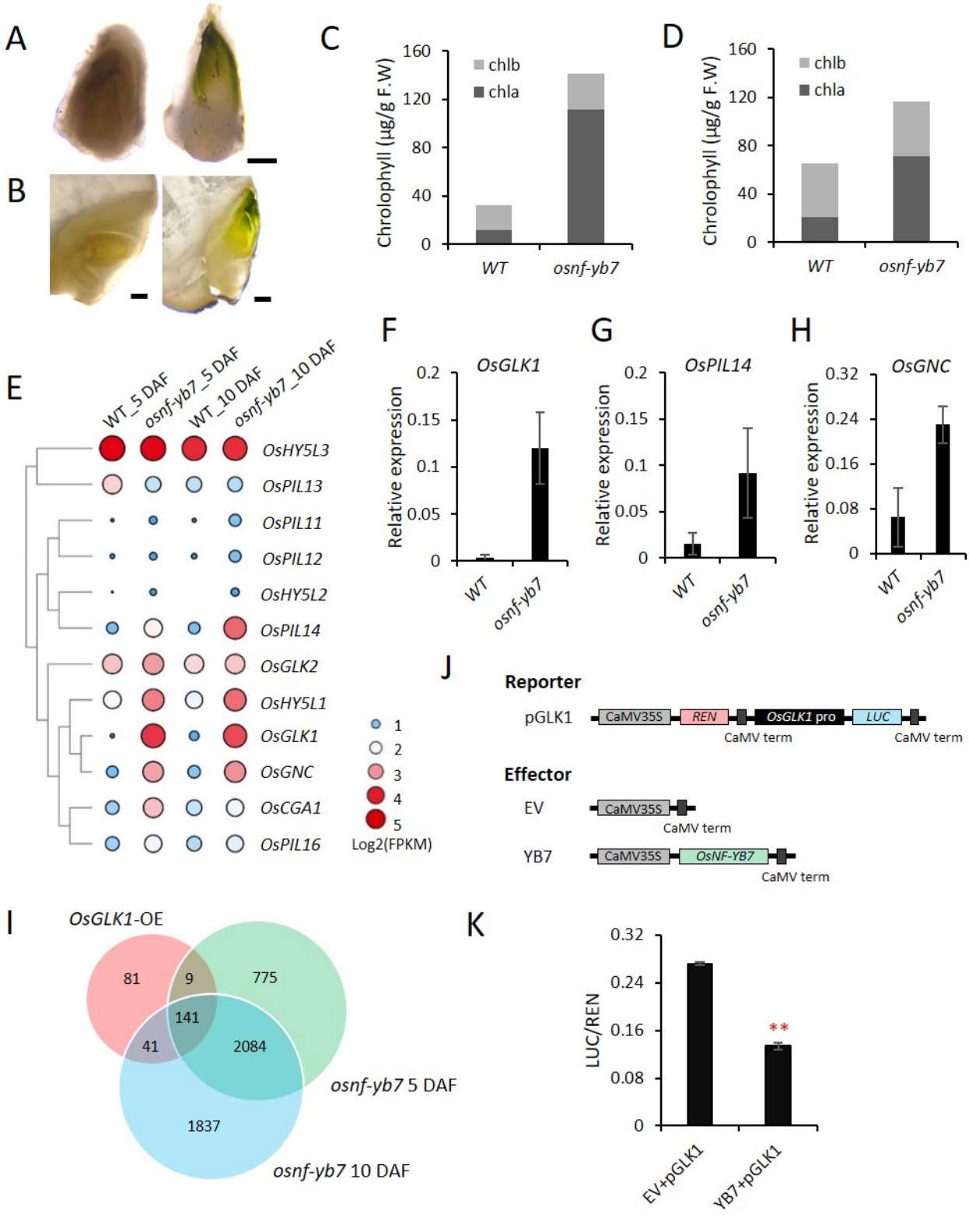

Figure 5. OsNF-YB7 negative regulates the expression of chlorophyll biogenesis-associated genes

(A, B). Embryo morphologies of the WT and *osnf-yb7* detached embryos at 8 DAF **(A)** and free-hand dissected embryos at maturation **(B)**. Scale bars = 0.2 mm.

(C, D). Chlorophyll levels in the WT and *osnf-yb7* embryos at ~15 DAF **(C)** and maturation **(D)**.

(E). Heat map of the expression of TFs associates with chlorophyll biogenesis or chloroplast development of the WT and *osnf-yb7*. The color dots indicate $\log_2$(RPKM mean) of the genes in three biological replicates.

(F–H). Expression of *OsGLK1* **(F)**, *OsPIL14* **(G)** and *OsGNC* **(H)** in WT and *osnf-yb7* at 5 DAF. The data are means ± SD of three biological replicates.

(I). The Venn diagram shows overlaps of the upregulated genes in the *osnf-yb7* embryos and in the *OsGLK1* overexpression transgenic plants (OsGLK1-OE). The upregulated genes in OsGLK1-OE were generated by Nakamura *et al.* (2009).

(J, K). Dual-luciferase reporter assays in rice protoplasts showing that OsNF-YB7 represses the activity of GLKpro::LUC. The constructs of reporter and effectors were shown in **(J)**. The data are means ± SD of three biological replicates. **, $p < 0.01$, as determined by Student's *t*-test.

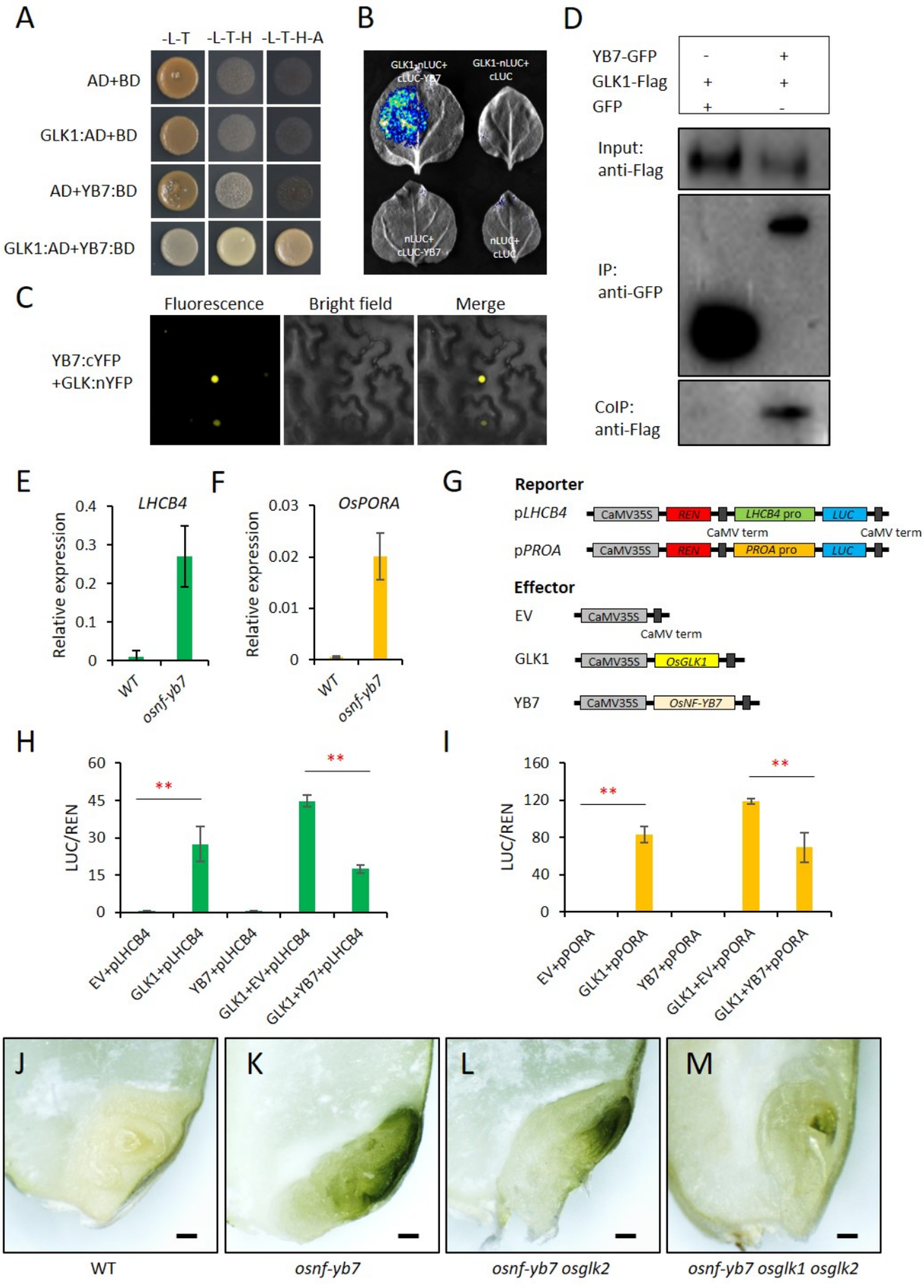

Figure 6. OsNF-YB7 interacts with OsGLK1 to repress the expression of *OsPORA* and *LHCB4*

(A). Y2H assays to test the interactions of OsNF-YB7 with OsGLK1. The indicated combinations of constructs were cotransformed into yeast cells and grown on the nonselective medium SD/-L-T and selective medium SD/-L-T-H and SD/-L-T-H-A.

(B). A split complementary luciferase (LUC) confirmed the interaction between OsNF-YB7 and OsGLK1. Coexpression of the fusion OsGLK1 and the N-terminal half of LUC (GLK1-nLUC) and the fusion of the C-terminal half of LUC and OsNF-YB7 (cLUC-YB7) in the epidermal cells of *N. benthamiana* leaves induced LUC activities, whereas the epidermal cells coexpressed OsGLK1-nLUC and cLUC, nLUC and cLUC-OsNF-YB7, or nLUC and cLUC did not show LUC activities.

(C). BiFC assays showed interactions between OsNF-YB7 and OsGLK1 in nuclei. OsGLK1 was fused with the N-terminal of yellow fluorescent protein (GLK1-nYFP); OsNF-YB7 was fused with the C-terminal of YFP (YB7-cYFP). The recombinant proteins were transiently coexpressed in leaf epidermal cells of *N. benthamiana.* Fluorescence signals indicate that OsGLK1 interacted with OsNF-YB7 in the nuclei.

(D). Co-IP assays showing that OsNF-YB7 interacts with OsGLK1 *in vivo*. 35S::OsNF-YB7:GFP (YB7-GFP) and 35S::OsGLK1:3xFlag (GLK-flag) were coexpressed in rice protoplasts and were immunoprecipitated with an anti-GFP antibody, and the immunoblots were probed with anti-GFP and anti-Flag antibodies. 35S::GFP (GFP) was a negative control.

(E, F). Expression of *LHCB4* **(E)** and *OsPORA* **(F)** was activated in the embryos of *osnf-yb7* at 10 DAF.

(G). Schematic diagrams of various constructs used in dual-luciferase reporter assays. LUC, firefly luciferase; REN, Renilla luciferase.

(H, I). Dual-luciferase reporter assays in rice protoplasts showing that OsNF-YB7 represses the activation of the *LHCB4pro::LUC* **(H)** and *PORApro::LUC* **(I)** reporters by OsGLK1. The LUC:REN ratio represents the LHCB4pro:LUC and PORApro:LUC activity relative to the internal control. Data are means ± SD of three biological replicates. **, $p < 0.01$, as determined by Student's *t*-test.

(J–M). Morphologies of the embryos produced by WT **(J)**, *osnf-yb7* **(K)**, *osnf-yb7;osglk2* double mutant **(L),** and *osnf-yb7;osglk1;osglk2* triple mutant **(M)**. Scale bars = 0.2 mm.

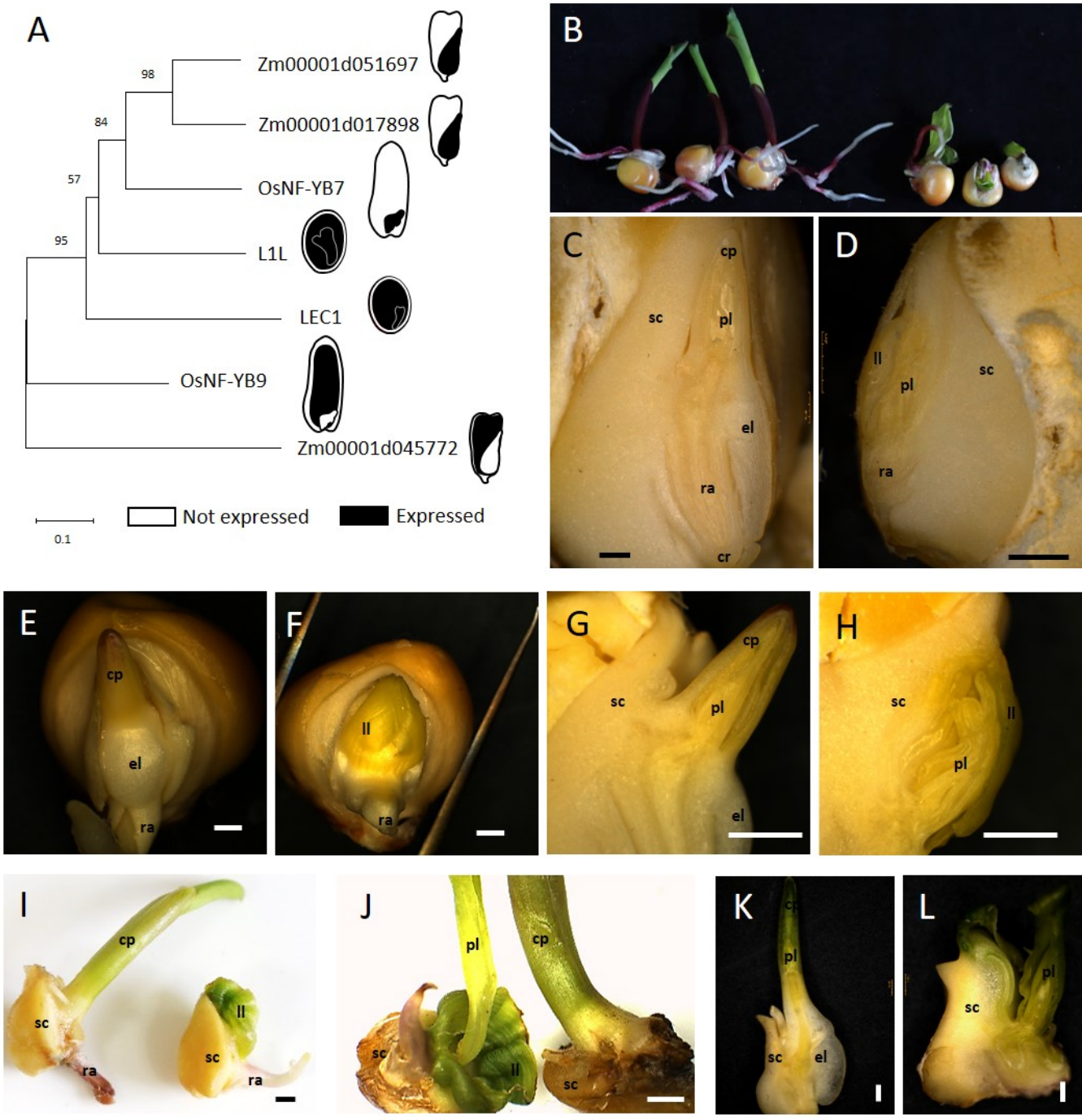

Figure 7. The maize OsNF-YB7 homologs play a similar role in embryo development

(A). The neighbor-joint tree and expressed preference of the LEC1-type genes in Arabidopsis, rice, and maize.

(B). Growth retardation showed in the maize *lec1* (double mutant of Zm00001d051697 and Zm00001d017898) mutant (right) when compared with the WT (left).

(C, D). Free-hand vertical sections of the mature WT **(C)** and maize *lec1* **(D)** embryos. Scale bars = 1 mm. Sc, scutellum; cp, coleoptile; el, epiblast-like structure; cr, coleorhiza; pl, plumule; ra, radicle; ll, leaf-like structure.

(E, F). The germinated embryos of WT **(E)** and maize *lec1* **(F)** after 3 d water imbibition. Scale bars = 1 mm. Cp, coleoptile; el, epiblast-like structure; ra, radicle; ll, leaf-like structure.

(G, H). Free-hand vertical sections of the germinated WT **(G)** and maize *lec1* **(H)** embryos after 48 h water imbibition. Scale bars = 1 mm. Sc, scutellum; cp, coleoptile; el, epiblast-like structure; pl, plumule; ll, leaf-like structure.

(I, J). The side view **(I)** and vertical view **(J)** of the detached germinated embryos of the WT and maize *lec1*. Scale bars = 1 mm. Sc, scutellum; cp, coleoptile; ra, radicle; ll, leaf-like structure.

(K, L). Free-hand vertical sections of the detached WT **(K)** and maize *lec1* **(L)** germinated embryos at 7 d after germination. Scale bars = 1 mm. Sc, scutellum; cp, coleoptile; el, epiblast-like structure; pl, plumule; ll, leaf-like structure.

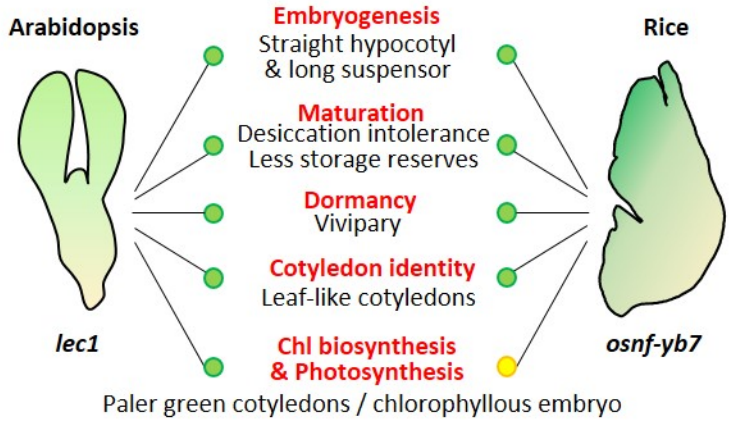

Figure 8. Schematic illustration of the functional conservation between Arabidopsis *LEC1* and rice *OsNF-YB7* for embryo development

Both Arabidopsis *lec1* and rice *osnf-yb7* mutants show defects of embryogenesis, maturation, and dormancy. Notably, like that observed in the *lec1* cotyledons, the embryonic envelope of *osnf-yb7* developed into a leaf-like structure with somewhat true-leaf identities. Additionally, the rice *osnf-yb7* develops chloroembryos, due to a chlorophyll-biogenesis activation in the embryo. However, the *lec1* seed showed paler green coloration than the WT.

Supplementary Files

This is a list of supplementary files associated with this preprint. Click to download.

- SupplementalFigures.pdf
- SupplementalTables.xlsx